Stability of rotating non-smooth complex fluids

Ishan Sharma

Journal of Fluid Mechanics / *FirstView* Article / August 2012, pp 1 - 29
DOI: 10.1017/jfm.2012.271, Published online:

J. Fluid Mech., page 1 of 29. © Cambridge University Press 2012
doi:10.1017/jfm.2012.271

Stability of rotating non-smooth complex fluids

Ishan Sharma†

Mechanics & Applied Mathematics Group, Department of Mechanical Engineering, Indian Institute of Technology Kanpur, Kanpur, Uttar Pradesh 208016, India

(Received 10 December 2011; revised 27 March 2012; accepted 5 June 2012)

We extend the classical energy criterion for stability, the Lagrange–Dirichlet theorem, to rotating non-smooth complex fluids. The stability test so developed is very general and may be applied to most rotating non-smooth systems where the spectral method is inapplicable. In the process, we rigourously define an appropriate coordinate system in which to investigate stability – this happens to be the well-known Tisserand mean axis of the body – as well as systematically distinguish perturbations that introduce angular momentum and/or jumps in the stress state from those that do not. With a view to future application to planetary objects, we specialize the stability test to freely rotating self-gravitating ellipsoids. This is then employed to investigate the stability to homogeneous perturbations of rotating inviscid fluid ellipsoids. We recover results consistent with earlier predictions, and, in the process, also reconcile some contradictory conclusions about the stability of Maclaurin spheroids. Finally, we consider the equilibrium and stability of freely rotating self-gravitating Bingham fluid ellipsoids. We find that the equilibrium shapes of most such ellipsoids are secularly stable to homogeneous perturbations that preserve angular momentum, but not otherwise. We also touch upon the effect of shear thinning on stability.

Key words: granular media, plastic materials, rotating flows

1. Introduction

Investigations into the shape of rotating self-gravitating homogeneous fluid ellipsoids have been carried out continuously since the time of Newton who, in contradistinction to Cassini posited that the Earth was flattened at the poles. Maclaurin later identified a class of oblate fluid ellipsoids that now carry his name. For a long time non-oblate shapes were thought to be impossible until Jacobi indicated that truly triaxial fluid ellipsoids can persist in equilibrium; this set of equilibrated shapes are now known as Jacobi ellipsoids that contain the Maclaurin spheroids as a special case. Dedekind, employing Dirichlet's equations describing homogeneously deforming self-gravitating inviscid fluids, found that it is possible that a rotating ellipsoid's shape be unchanging, in spite of coaxial internal vortical motion; this defines the Dedekind equilibrium sequence. Later, Riemann identified all possible scenarios when a rotating fluid ellipsoid retains its shape; these are the Riemann ellipsoids that have the Jacobi and Dedekind ellipsoids as particular instances. For a more detailed history of the subject we direct the interested reader to Chandrasekhar (1969). Investigations into non-ellipsoidal shapes and/or inhomogeneous fluid masses due to Lyapunov, Poincare,

† Email address for correspondence: ishans@iitk.ac.in

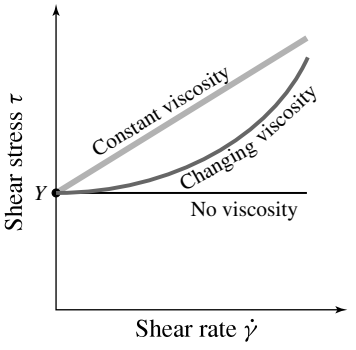

FIGURE 1. Examples of non-smooth rheological responses in one dimension. The fluid remains rigid until the shears stress exceeds Y, beyond which it may flows as a fluid with no, constant or changing viscosity. The non-smoothness is due to the discontinuity in slope at the yield point.

Darwin, Jeans, Leichtenstein and others are documented in Jardetzky (1958) and Hagihara (1970).

In contrast to the question relating to their equilibrium shapes, enquiries into the stability of shapes did not commence until Riemann (1860). Riemann, employing the Lagrange–Dirichlet theorem, a particular case of the energy criterion, cf. § 4, and Dirichlet's framework for homogeneously deforming ellipsoids, investigated the stability of the Riemann ellipsoids. Riemann showed, for example, that the Maclaurin spheroids were secularly stable for axes ratios $\beta = a_3/a_1$ greater than $\beta_R = 0.3033$. Here we recall that systems found stable by Lagrange–Dirichlet theorem are labelled secularly stable. On its face Riemann's result appears surprising, as it ignores the bifurcation of the Jacobi ellipsoids from the Maclaurin sequence when β equals $\beta_J = 0.5827$. In fact, later, Jeans (1961, p. 213) and Lyttleton (1953, p. 45) demonstrated that the Lagrange–Dirichlet stability criterion applied directly to the Navier–Stokes equations predicts that Maclaurin spheroids with axes ratio beyond β_J are secularly stable. However, no comment is made about why these results are at variance with Riemann's. Chandrasekhar, along with Lebovitz in the 1960s, employed moments of the Navier–Stokes equation, the so-called virial method, to investigate rotating fluid ellipsoids in a unified manner; much of this work is collected together in Chandrasekhar (1969). They followed a spectral method to identify exponentially growing eigenmodes and thereby probe the stability of these ellipsoids. In particular, they confirmed the results of Jeans and Lyttleton, but also showed that for axes ratios between β_R and β_J, inviscid Maclaurin ellipsoids were ordinarily stable. We note that systems found stable by a spectral analysis are said to be ordinarily stable. Again, no reason as to why Riemann predicts secular stability for $\beta > \beta_R$ was provided. Stability to perturbations of higher modes were investigated by Poincare, Lyapunov, Jeans, Darwin, Cartan, Chandrasekhar and others, by both energy and spectral methods, and excellent accounts are available in the monographs by Lyttleton (1953) and Chandrasekhar (1969). In spite of its antiquity, the equilibrium, stability and dynamics of rotating fluid masses continues to be an active research field; see, e.g., Lebovitz (1998).

We are interested in the stability of rotating complex fluid ellipsoids that follow a non-smooth rheology. Several examples of non-smooth constitutive responses in one dimension are shown in figure 1. Our investigation is motivated by the growing

interest in the origins and dynamics of minor planets such as asteroids and small moons. Several of the near-Earth asteroids and recently discovered small moons of the giant planets are suspected to be granular aggregates held together by their own gravity; see, e.g., Richardson *et al.* (2002). In fact, most smaller main belt asteroids with diameters less than 50 km may also be rubble piles; see, e.g., Bottke *et al.* (2002). Granular aggregates remain immobile at low stresses, but begin to flow at higher loads, and are often approximated by non-smooth constitutive laws. Indeed, Jop, Forterre & Pouliquen (2006) have suggested that Bingham fluids in which both the viscosity and the yield stress depend on the local pressure are good models for granular aggregates as they transition from a solid-like phase to begin flowing slowly.

A non-smooth rheology precludes stability analysis by the spectral method. We, therefore, extend the classical energy criterion for stability, the Lagrange–Dirichlet theorem, to rotating systems displaying a non-smooth constitutive response. Special care is taken to account for the body's rotation and its non-smoothness and this leads us to define an appropriate coordinate system in which to investigate stability – this turns out to be the familiar *Tisserand's mean axis of the body* – as well as to systematically differentiate perturbations that do not preserve angular momentum and/or introduce jumps in the stress state from those that do. The stability test so developed is sufficiently general to be applicable to any rotating non-smooth continuous system perturbed by any kinematically permitted perturbation. Here, for simplicity, we specialize our stability test to homogeneous perturbations, i.e., perturbation modes wherein the body deforms homogeneously, and consider first inviscid fluid ellipsoids. We recover results consistent with those of Jeans, Lyttleton and Chandrasekhar, and, in the process, clarify the reasons behind Riemann's apparently incompatible predictions about the stability of Maclaurin spheroids. Finally, we consider the stability of freely rotating self-gravitating Bingham fluid ellipsoids as an example of our stability criterion's ability to address non-smooth systems. As we discuss in greater detail in § 3.2, Bingham fluids remain rigid until the stress state violates a yield condition; see figure 2. This example also serves as a first step towards analysing the stability of granular planetary objects; actual application to asteroids will be pursued elsewhere.

We next develop equations that govern homogeneous deformations of ellipsoids. These will be employed to first identify equilibrium regions for rotating self-gravitating fluid ellipsoids and, then, to investigate their stability to homogeneous perturbations.

2. Homogeneous dynamics

Equations governing the dynamics of a homogeneously deforming uniform fluid ellipsoid have been developed by Riemann, Lebovitz, Chandrasekhar and others; see Chandrasekhar (1969). These were extended to granular aggregates by Sharma, Jenkins & Burns (2009). We summarize the derivation for completeness, and more details may be found in Sharma *et al.* (2009).

Consider a coordinate system $\mathscr{O}$ rotating at a possibly time-varying rate $\boldsymbol{\omega}(t)$. With $\boldsymbol{\omega}$ we identify an antisymmetric angular velocity tensor $\boldsymbol{\Omega}$ such that for any vector $\boldsymbol{a}$,

$$\boldsymbol{\omega} \times \boldsymbol{a} = \boldsymbol{\Omega} \cdot \boldsymbol{a}; \tag{2.1}$$

correspondingly $\boldsymbol{\omega}$ is $\boldsymbol{\Omega}$'s *axial vector*. The linear momentum balance in $\mathscr{O}$ is

$$\boldsymbol{\nabla} \cdot \boldsymbol{\sigma} + \rho \left(\boldsymbol{b} - \dot{\boldsymbol{\Omega}} \cdot \boldsymbol{x} - \boldsymbol{\Omega}^2 \cdot \boldsymbol{x} - 2\boldsymbol{\Omega} \cdot \boldsymbol{v} \right) = \rho \dot{\boldsymbol{v}}, \tag{2.2}$$

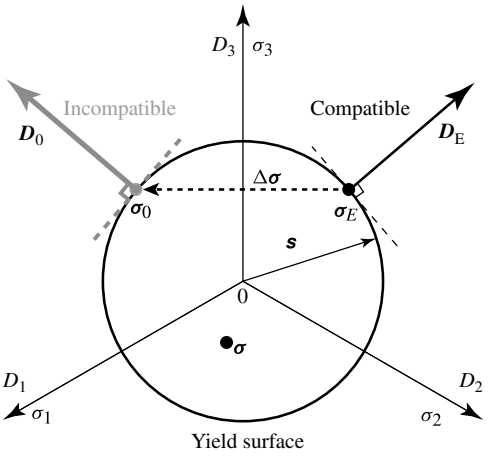

FIGURE 2. The yield surface of a Bingham fluid appears as a circle of radius $|\boldsymbol{s}|$ when viewed along the pressure axis $\sigma_1 = \sigma_2 = \sigma_3$ in principal stress/strain space. The point marked $\boldsymbol{\sigma}_E$ corresponds to the stress state at equilibrium. The strain rate $\boldsymbol{D}_E$ compatible with $\boldsymbol{\sigma}_E$ is normal to the yield surface at E. In case the incompatible strain rate $\boldsymbol{D}_0$ shown by the grey vector is superimposed by a perturbation, the equilibrium stress state immediately shifts to a location $\boldsymbol{\sigma}_0$ on the yield surface where the imposed strain rate would be compatible. This leads to jump $\Delta\boldsymbol{\sigma}$ in the stress state. Also shown is an arbitrary stress state $\boldsymbol{\sigma}$ that may lie within or on the yield surface.

where $\boldsymbol{\sigma}$ is the stress tensor, ρ is the density, $\boldsymbol{b}$ is the body force, $\boldsymbol{x}$ is a material element's location, $\boldsymbol{v}$ is the material element's velocity relative to $\mathscr{O}$, and all time derivatives here and henceforth will be in the rotating frame $\mathscr{O}$. Taking the tensor product of the above equation with $\boldsymbol{x}$ and integrating over the body's volume V, we obtain after utilizing Green's theorem that

$$-\overline{\boldsymbol{\sigma}}V + \boldsymbol{M}^{\mathrm{T}} - \left(\dot{\boldsymbol{\Omega}} + \boldsymbol{\Omega}^2\right) \cdot \boldsymbol{I} + 2\boldsymbol{\Omega} \cdot \int \rho \boldsymbol{v} \otimes \boldsymbol{x}\, \mathrm{d}V = \int \rho \boldsymbol{v} \otimes \dot{\boldsymbol{x}}\, \mathrm{d}V, \tag{2.3}$$

where we recall that the tensor product between vectors $\boldsymbol{a}$ and $\boldsymbol{b}$ is denoted by $\boldsymbol{a} \otimes \boldsymbol{b}$ with $(\boldsymbol{a} \otimes \boldsymbol{b})_{ij} = a_i b_j$,

$$\overline{\boldsymbol{\sigma}} = \frac{1}{V} \int \boldsymbol{\sigma}\, \mathrm{d}V \tag{2.4}$$

is the average stress within the body,

$$\boldsymbol{I} = \int \rho \boldsymbol{x} \otimes \boldsymbol{x}\, \mathrm{d}V \tag{2.5}$$

is the inertia tensor,

$$\boldsymbol{M} = \int \rho \boldsymbol{x} \otimes \boldsymbol{b}\, \mathrm{d}V \tag{2.6}$$

is the body-force moment tensor, and we have set the terms involving surface traction to zero preempting our application to bodies with free surface. Two comments are in order. First, the inertia tensor $\boldsymbol{I}$ should be compared with the commonly employed Euler's moment of inertia tensor $\boldsymbol{J}$ in rigid body dynamics, cf. (4.4). Second, the

torque, which is the cross-product of the force with its moment arm, is related to the axial vector corresponding to $\boldsymbol{M}$'s antisymmetric part.

We now restrict ourselves to homogeneous deformations, wherein the relative velocity

$$\boldsymbol{v} = \boldsymbol{L} \cdot \boldsymbol{x}, \tag{2.7}$$

in terms of the velocity gradient $\boldsymbol{L}(t)$ that depends only on time, but not $\boldsymbol{x}$. Furthermore, we will here focus on isolated ellipsoidal bodies with uniform density, so that the only external force is due to the body's self-gravity. The ellipsoid's semi-major axes are taken to be $a_1 \geqslant a_2 \geqslant a_3$, while the axes ratios are $\alpha = a_2/a_1$ and $\beta = a_3/a_1$. The gravitational force per unit mass at a location $\boldsymbol{x}$ within such an ellipsoid is

$$\boldsymbol{b} = -2\pi\rho G \boldsymbol{A} \cdot \boldsymbol{x}, \tag{2.8}$$

where G is the universal constant of gravitation, and $\boldsymbol{A}$ is a shape tensor that captures the effect of the ellipsoidal shape on its internal gravitational field; see, e.g., Kellogg (1953, p. 194). The tensor $\boldsymbol{A}$ is diagonalized in the ellipsoid's principal axes system with

$$A_1 = A_2 = -\frac{\beta^2}{1-\beta^2} + \frac{\beta}{(1-\beta^2)^{3/2}} \sin^{-1}\sqrt{1-\beta^2} \tag{2.9}$$

for oblate ellipsoids. For prolate objects ($1 > \alpha = \beta$),

$$A_2 = A_3 = \frac{1}{1-\beta^2} - \frac{\beta^2}{2\,(1-\beta^2)^{3/2}} \ln\left(\frac{1+\sqrt{1-\beta^2}}{1-\sqrt{1-\beta^2}}\right), \tag{2.10}$$

and, finally, for truly triaxial ellipsoids ($1 > \alpha > \beta$)

$$A_1 = \frac{2\alpha\beta}{(1-\alpha^2)\sqrt{1-\beta^2}}\left(F[r,s] - E[r,s]\right) \tag{2.11a}$$

and

$$A_3 = \frac{2\alpha\beta}{(\alpha^2-\beta^2)\sqrt{1-\beta^2}}\left(\frac{\alpha}{\beta}\sqrt{1-\beta^2} - E[r,s]\right), \tag{2.11b}$$

where F and E are, respectively, elliptic integrals of the first and second kinds with argument $r = \sqrt{1-\beta^2}$ and parameter $s = \sqrt{(1-\alpha^2)/(1-\beta^2)}$; see, e.g., Abramowitz & Stegun (1965, p. 587). In each case, we provide only two of the A_i, with the third component calculated from

$$A_1 + A_2 + A_3 = 2; \tag{2.12}$$

see Chandrasekhar (1969, p. 54, equation (108)). Employing $\boldsymbol{b}$ from (2.8) in (2.6) we find that

$$\boldsymbol{M} = -2\pi\rho G \boldsymbol{A} \cdot \boldsymbol{I}. \tag{2.13}$$

Utilizing this in (2.3) we find that

$$-\overline{\boldsymbol{\sigma}} V - \left(2\pi\rho G \boldsymbol{A} + \dot{\boldsymbol{\Omega}} + \boldsymbol{\Omega}^2 + 2\boldsymbol{\Omega} \cdot \boldsymbol{L}\right) \cdot \boldsymbol{I} = \left(\dot{\boldsymbol{L}} + \boldsymbol{L}^2\right) \cdot \boldsymbol{I}. \tag{2.14}$$

In the above equation, the terms $-\dot{\boldsymbol{\Omega}} \cdot \boldsymbol{I}$, $-\boldsymbol{\Omega}^2 \cdot \boldsymbol{I}$ and $-2\boldsymbol{\Omega} \cdot \boldsymbol{L} \cdot \boldsymbol{I}$ represent contributions from, respectively, the rotational inertia, centrifugal and Coriolis forces. The rate of

change of the inertia tensor $\dot{\boldsymbol{I}}$ may be obtained by differentiating (2.5) and employing (2.7), to find

$$\dot{\boldsymbol{I}} = \boldsymbol{L}\cdot\boldsymbol{I} + \boldsymbol{I}\cdot\boldsymbol{L}^{\mathrm{T}}. \tag{2.15}$$

We emphasize that the development so far has been independent of material properties. Given an appropriate rheology relating $\boldsymbol{\sigma}$ to deformation and/or its rate, the above equations follow the dynamics of a homogeneously deforming self-gravitating uniform ellipsoid.

3. Equilibrium shapes

A rotating ellipsoid's equilibrium may be defined as one in which the ellipsoid's shape remains unchanging, i.e., externally the ellipsoid appears to rotate rigidly at a constant rate. This, however, does not preclude the possibility that the material within the ellipsoid may be rotating at a rate different from that of the ellipsoid's principal axes. In fact, in inviscid fluids wherein vortical motion may be sustained indefinitely, this leads to a class of equilibrium solutions known collectively as Riemann ellipsoids, see, e.g., Chandrasekhar (1969, p. 129). Because we ultimately aim to address dissipative fluids wherein persistent vortical motion is impossible at equilibrium, we henceforth ignore this alternative, assuming that, at equilibrium, an observer rotating with the ellipsoid's shape's principal axes will find material points at rest.

To identify equilibrium shapes, we align the coordinate frame $\mathscr{O}$ with the equilibrated ellipsoid's principal axes assuming them to rotate at a rate $\boldsymbol{\omega}_E = \omega_E\hat{\boldsymbol{e}}_3$ about the ellipsoid's axis of maximum inertia. This latter choice is prompted by the knowledge that in the presence of any dissipation, freely tumbling bodies ultimately align into a state of pure rotation about their axis of maximum inertia; see, e.g., the general discussion in Greenwood (1988, p. 408) and quantitative formulations in the context of planetary bodies by Burns & Safronov (1973) and Sharma, Burns & Hui (2005). Given this choice of $\mathscr{O}$ and the preceding discussion, $\boldsymbol{L} = \dot{\boldsymbol{L}} = 0 = \dot{\boldsymbol{\Omega}}$ at equilibrium, and (2.14) reduces to

$$\overline{\boldsymbol{\sigma}}_E V = -\left(\boldsymbol{A} + \boldsymbol{\Omega}_E^2\right)\cdot\boldsymbol{I}, \tag{3.1}$$

where time is scaled by $1/\sqrt{2\pi\rho G}$ and the subscript 'E' identifies quantities at equilibrium. With an eye to the stability analysis to follow, we explicitly identify only those quantities that change instantaneously following a velocity perturbation; other quantities, such as volume V, will be assumed to take their equilibrated values. Non-dimensionalizing stress by $(3/20\pi)(2\pi\rho G m)\,(4\pi/3V)^{1/3}$, we find that

$$\left.\begin{aligned} &\overline{\sigma}_{11} = \left(\omega_E^2 - A_1\right)(\alpha\beta)^{-2/3}, \quad \overline{\sigma}_{22} = \alpha^2\left(\omega_E^2 - A_2\right)(\alpha\beta)^{-2/3}, \quad \text{and} \\ &\overline{\sigma}_{33} = -\beta^2 A_3(\alpha\beta)^{-2/3} \end{aligned}\right\} \tag{3.2}$$

are the stress components in $\mathscr{O}$. Note the absence of shear stresses.

Depending on the ellipsoid's constituent material the average stress computed above cannot assume all values; they will be constrained by yield conditions appropriate to the material. We explore this in the context of two very different fluids.

3.1. *Newtonian fluids*

The stress tensor in inviscid incompressible fluids is simply $\boldsymbol{\sigma} = -p\mathbf{1}$, where the pressure $p = -\mathrm{tr}(\boldsymbol{\sigma})/3$. Averaging over the volume provides $\overline{\boldsymbol{\sigma}} = -\bar{p}\mathbf{1}$. Thus, the stress

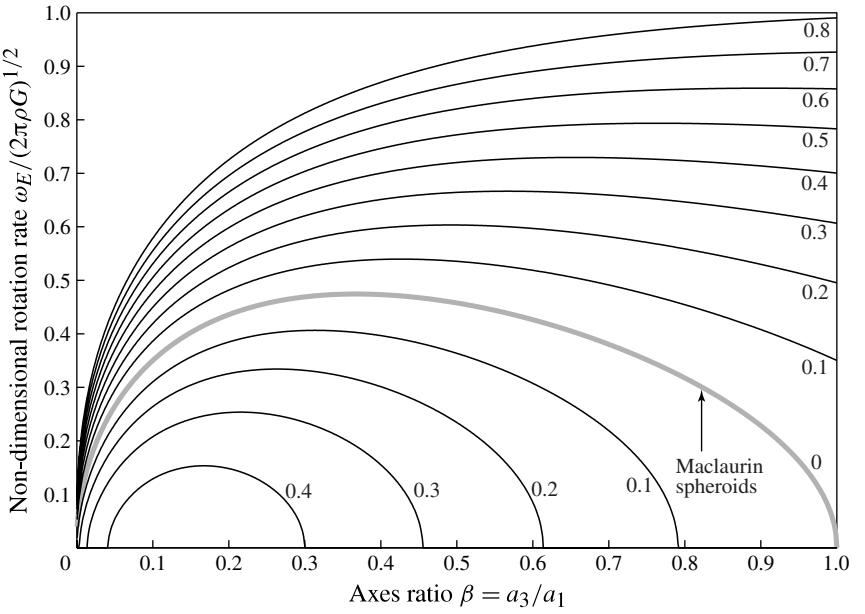

FIGURE 3. Equilibrium regions for oblate Bingham fluid ellipsoids with $\alpha = 1$. The critical curves are identified by the corresponding Bingham yield stress Y.

components evaluated above are all equal, providing the relationships

$$\omega_E^2 - A_1 = \alpha^2 \left(\omega_E^2 - A_2\right) = -\beta^2 A_3 = -\overline{p}_E (\alpha\beta)^{2/3}. \tag{3.3}$$

Given A_i's dependence on the axes ratios, the above balances help us relate the equilibrated ellipsoid's shape to its rotation rate at equilibrium.

Consider first the possibility of a spheroidal form wherein $a_1 = a_2 > a_3$, i.e., $\alpha = 1 > \beta$. Thus, $A_1 = A_2$, and we find that an inviscid fluid self-gravitating rotating spheroid will be in equilibrium if

$$\omega_E = \left(A_1 - \beta^2 A_3\right)^{1/2}. \tag{3.4}$$

Because A_1 and A_3 are expressible in terms of β from (2.9), the above defines the heavy grey curve in the shape–spin (β–ω_E) space of figure 3; these are the Maclaurin spheroids. Only those oblate fluid ellipsoids that lie on this curve will persist in equilibrium.

Next, we explore the possibility of prolate ellipsoidal shapes at equilibrium. Setting $a_1 > a_2 = a_3$, i.e. $1 > \alpha = \beta$ in (3.3) and utilizing (2.10) we find that proloidal shapes are not possible for fluids. Finally, if $a_1 > a_2 > a_3$, i.e., $1 > \alpha > \beta$, combining (3.3) with the formulae for A_i in (2.11), we find that truly triaxial ellipsoidal shapes are indeed possible for fluids provided that

$$\omega_E = \left\{ \frac{A_1(\alpha, \beta_J) - \alpha^2 A_2(\alpha, \beta_J)}{1 - \alpha^2} \right\}^{1/2}, \tag{3.5}$$

where β_J is the solution to the nonlinear equation

$$\beta = \frac{\alpha}{\sqrt{1-\alpha^2}}\left(\frac{A_2 - A_1}{A_3}\right)^{1/2}. \tag{3.6}$$

This defines a curve in the three-dimensional shape–spin $(\alpha, \beta, \omega_E)$ space on which lie the Jacobi ellipsoids.

The analysis above thus recovers classically known results; see, e.g., Chandrasekhar (1969). Note that given an ellipsoidal shape, a fluid body can sustain only a unique rotation rate at equilibrium. This is because fluids cannot resist shear in the absence of differential motion. We next consider a class of fluids that, even in the absence of differential motion, have finite shear resistance.

3.2. *Bingham fluids*

Bingham fluids are characterized by their ability to support shear stresses until some critical value is reached whereupon they yield and begin flowing as a fluid. Oldroyd (1947) and Prager (1961, p. 136) put forward three-dimensional constitutive relationships for Bingham fluids. The material is assumed rigid until it violates the yield condition

$$|\boldsymbol{s}| \leqslant Y, \tag{3.7}$$

where

$$\boldsymbol{s} = \boldsymbol{\sigma} + p\mathbf{1}, \tag{3.8}$$

is the deviatoric stress tensor, $|\boldsymbol{s}| = \sqrt{s_{ij}s_{ij}}$ is a measure of $\boldsymbol{s}$'s magnitude, and Y is the Bingham yield stress that is assumed constant. Post-yield, the deviatoric stress

$$\boldsymbol{s} = Y\frac{\boldsymbol{D}}{|\boldsymbol{D}|}, \tag{3.9}$$

where $\boldsymbol{D}$ is the flow's stretching rate after yielding and, without loss of generality, we assume that viscosity is absent. Viscosity's presence does not change either the equilibrium's location or its secular stability; see, e.g., Ziegler (1968, p. 91). The black curve in figure 1 depicts this rheology in one dimension.

While the formal derivation is available in Oldroyd (1947) or Prager (1961), we discuss the key idea underlying (3.9). The constitutive relation (3.9) is obtained by assuming that strain rates after yielding are normal to the yield surface. For example, the strain rate post-yield $\boldsymbol{D}_E$ when the stress state coincides with $\boldsymbol{\sigma}_E$ in figure 2 is restricted to be along the normal at that location; such a strain rate is said to be compatible. Taking the gradient of (3.7) now provides a flow rule

$$\boldsymbol{D} = \dot{q}\boldsymbol{s} \tag{3.10}$$

in terms of a proportionality constant $\dot{q}$ that relates the strain rate after yielding in terms of the deviatoric stress at yield. Combining (3.10) and (3.7) furnishes (3.9). The normality assumed above is a consequence of the maximum dissipation postulate; see, e.g., Lubliner (1990, p. 117). Referring again to figure 2, this postulate hypothesizes that $(\boldsymbol{\sigma} - \boldsymbol{\sigma}_E) : \boldsymbol{D}_E \geqslant 0$, where for two tensors $\boldsymbol{B}$ and $\boldsymbol{C}$, $\boldsymbol{B} : \boldsymbol{C} = B_{ij}C_{ji}$. Taking $\boldsymbol{\sigma}$ infinitesimally close to $\boldsymbol{\sigma}_E$ and on the yield surface, we obtain the equivalent statement that during yielding the incremental work $d\boldsymbol{\sigma}_E : \boldsymbol{D}_E$ is always positive. Because $d\boldsymbol{\sigma}_E$ is tangent to the yield surface at the location E, we recover normality of the post-yield strain rate $\boldsymbol{D}_E$ at E. This postulate is often invoked when modelling materials displaying distinct constitutive responses separated by a yield surface.

Finally, we make two additional comments. First, we note that flowing Bingham fluids dissipate energy. However, in contrast to viscous dissipation, the dissipative terms $\boldsymbol{D}/|\boldsymbol{D}|$ is rate independent and should be compared with dry friction. Second, while it is impossible to find the stress tensor everywhere within a rigid body, say, e.g., within the Bingham fluid prior to yielding, the volume-averaged stress is exactly known from (3.1), and in the following we employ the constitutive relationships after averaging.

A Bingham fluid ellipsoid will be in equilibrium as long as the yield condition (3.7) is not violated. This inequality delineates a region in the three-dimensional α–β–ω_E space that is bound by an upper and a lower critical surface obtained by combining the yield condition (3.7) at equality with the average stress obtained from (3.1):

$$\omega_E^2 = \frac{1}{2(1-\alpha^2+\alpha^4)}\left\{(2-\alpha^2)A_1 - \alpha^2(1-2\alpha^2)A_2 - \beta^2(1+\alpha^2)A_3 \pm \sqrt{3d}\right\}, \quad (3.11)$$

where

$$d = 2(1-\alpha^2+\alpha^4)\,(\alpha\beta)^{4/3}\,Y^2 - \left\{\alpha^2(A_1-A_2) + (1-\alpha^2)\beta^2 A_3\right\}^2, \quad (3.12)$$

and the Bingham yield stress Y has been scaled by $(3/20\pi)(2\pi\rho Gm)\,(4\pi/3V)^{1/3}$. When Y is zero, we retrieve the case of inviscid fluids. Then, for d to be non-negative, it is necessary that either $\alpha = 1$ and we recover the Maclaurin spheroids, or β satisfies (3.6) corresponding to the Jacobi ellipsoids.

To gain insight into this three-dimensional equilibrium landscape, we, once again, consider oblate, prolate and triaxial shapes in turn; this corresponds to taking appropriate two-dimensional slices. Setting $\alpha = 1$ and $A_1 = A_2$ in (3.11), we find that oblate Bingham fluid ellipsoids with yield stress Y may reside in equilibrium within the region in ω_E–β space bound by the two critical curves

$$\omega_E^2 = A_1 - \beta^2 A_3 \pm \sqrt{\tfrac{3}{2}}\,\beta^{2/3} Y; \quad (3.13)$$

note that the lower curve may not exist for all Y. Figure 3 displays the equilibrium regions for several values of Y. At fixed β, crossing the upper critical curve leads to yielding due to excessive centrifugal stresses, while the lower critical curve corresponds to an inability to support equatorial gravitational stress at low rotation rates.

Proloidal equilibrium shapes are obtained by taking $\alpha = \beta$ and $A_2 = A_3$ in (3.11). The resulting equilibrium zones for various values of Y are shown in figure 4. Note that while inviscid fluid ellipsoids could not exist, a non-vanishing yield stress allows proloidal equilibrium shapes. Finally, figure 5 shows the equilibrium landscape for 'average' triaxial ellipsoids satisfying $\alpha = (1+\beta)/2$. As $Y \to 0$, the equilibrium zones shrink to a point that represents the intersection of the inviscid Jacobi sequence of ellipsoids with the plane $\alpha = (1+\beta)/2$.

The equilibrium analysis of this section mirrors closely work done in the context of rubble pile asteroids by Holsapple (2001, 2007) and Sharma *et al.* (2009); see also Harris, Fahnestock & Pravec (2009). Granular aggregates are often modelled via pressure-dependent yield surfaces, e.g., the Drucker–Prager yield criterion, that lead to post-yield stresses very similar to (3.9); see, e.g., Chen & Han (1988, p. 94). The ensuing equilibrium landscape for oblate, prolate and average triaxial ellipsoids is similar to figures 3–5; see figures 3 and 4 of Sharma *et al.* (2009) and figure 7 of Holsapple (2007). Complementary computational work employing hard- and soft-particle discrete-element methods was done by, respectively, Richardson, Elankumaran

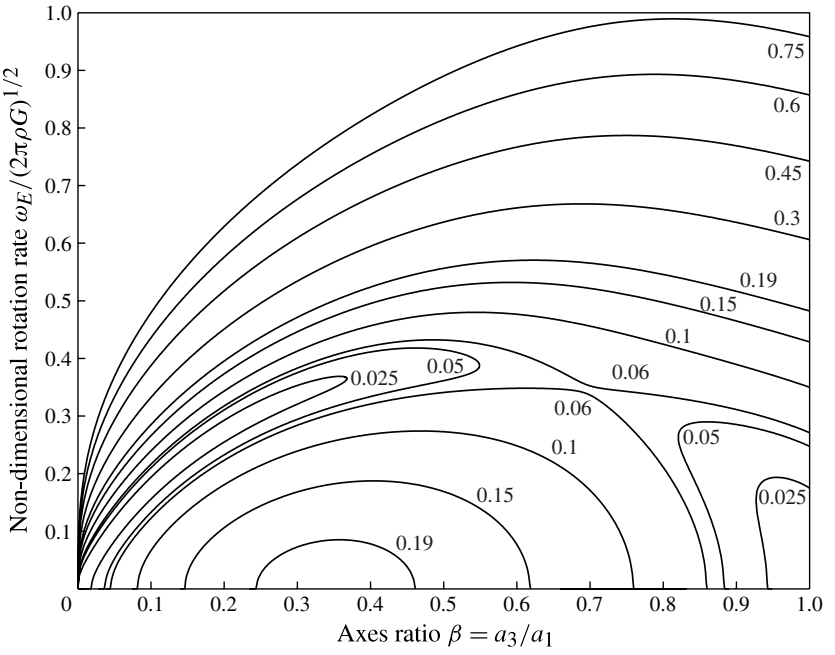

FIGURE 4. Equilibrium regions for prolate Bingham fluid ellipsoids with $\alpha = \beta$; cf. figure 3.

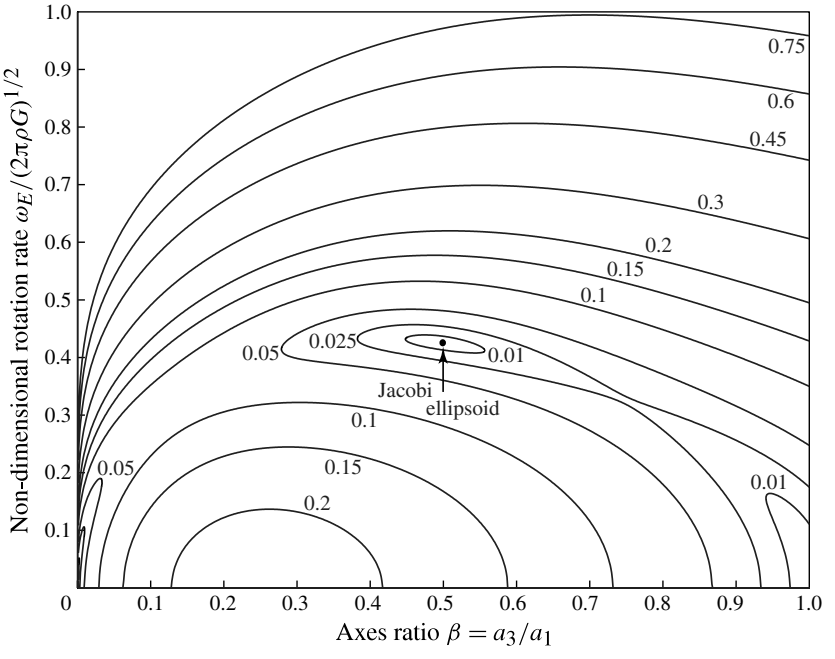

FIGURE 5. Equilibrium regions for average triaxial Bingham fluid ellipsoids with $\alpha = (1 + \beta)/2$; cf. figure 3.

& Sanderson (2005) and Sanchez & Scheeres (2012). Sharma *et al.* (2009) and Sanchez & Scheeres (2012) show that results obtained via homogeneous dynamics matched computational results well, and this engenders confidence in our predicting failure on the basis of a volume-averaged stress field.

We now proceed to investigate the stability of these equilibrium regions.

4. Stability criterion

Lyapunov's definition of local stability requires that small perturbations of a system lead to small departures of the system's coordinates from their equilibrium values; see, e.g., LaSalle & Lefschetz (1961, p. 28). There are fundamentally two methods of testing local stability: Lyapunov's first method also referred to as the linear stability/spectral analysis, and the energy criterion whose classical version is the Lagrange–Dirichlet theorem. Depending on the approach employed, a system is said to be spectrally/ordinarily or, respectively, energetically/secularly stable/unstable. The former proceeds by linearizing the governing dynamical equations about the equilibrium point and then finding the growth/decay rates of the linearized system's eigenmodes as determined by the associated eigenvalues. It is necessary, therefore, that the system's governing equations be amenable to linearization. Given this requirement, it is not possible to investigate the stability of systems having non-smooth constitutive behaviours via a spectral analysis.

The energy criterion's classical version is the Lagrange–Dirichlet theorem:

(i) *a conservative system's equilibrium is stable if the system's total potential energy is minimized in that configuration.*

For non-smooth dissipative systems an alternative incremental form is more useful:

(ii) *a system's equilibrium state is stable if during a kinematically permissible infinitesimal displacement the work done on the system by external agencies is less than the total energy stored and/or dissipated by the system.*

Statement (i) may be obtained as a special case of (ii) by adopting a strain energy function and appropriate force potentials as is possible for conservative systems; cf. § 4.2. As stated, the energy criterion is applicable to systems that are stationary at equilibrium. However, by a judicious application of D'Alembert's principle it is possible to reduce a system's dynamical configuration to rest; we did so when writing (2.2). In that case, inertial forces are considered as external forces.

In finite dimensions, under appropriate conditions, both local stability tests noted above ensure the system's local stability in the sense of Lyapunov; see, e.g., Ziegler (1968). These tests may not, however, be directly ported to continuous systems; see, e.g., Movchan (1959, 1960) or Knops & Wilkes (1966, 1973). We will not explore this further as, ultimately, we will consider dynamical evolution only in the space of homogeneous deformations that constitutes a finite-dimensional system. The reader interested in conservative/dissipative continuous systems may refer to texts such as Nguyen (2000) or Koiter (2008). Finally, note that in finite dimensions secularly stable systems are also spectrally stable, but the converse may not always hold. In particular, gyroscopic forces may stabilize systems in conditions wherein the energy test predicts instability; see Ziegler (1968, p. 73).

Before formulating the energy criterion in the context of freely rotating deformable bodies, it is necessary to discuss the coordinate system's role in a stability analysis.

4.1. *Coordinate system*

Lyapunov's definition requires measuring the departure of the system's coordinates from equilibrium. Therefore, to avoid unphysical results in case of systems that are perturbed from a dynamical configuration it is necessary that the system's coordinates be measured in an appropriately moving frame. For example, a rotating rigid body viewed from a fixed coordinate system will always be reported as unstable, as the body's rotation will carry every material point far away from its initial location. A coordinate system aligned with the body's principal axes of inertia rectifies this problem for rigid objects, but may not always be satisfactory for deformable bodies. For example, the fluid Dedekind ellipsoids discussed in the Introduction will have uniform relative vorticity in a coordinate system aligned with the ellipsoid's principal axes. This rotating coordinate system, thus, suffers from the same drawback as that of a fixed frame.

Deformable rotating systems conserve angular momentum by modifying their spins to compensate not only for the action of external torque, but also changes in inertia. This was exemplified in the context of a freely rotating gaseous mass by Schwarzschild in 1897; see the discussion in Jeans (1961, article 183, p. 199). Because post-perturbation the freely rotating gaseous mass conserves angular momentum, any change in its shape, and consequently its moment of inertia, is compensated for by appropriately adapting the rotation rate. So, for example, if the rotating mass flattens in a plane orthogonal to the spin axis, its rotation rate will decrease. Consequently, if the stability analysis were carried out in a coordinate system whose rotation rate remains fixed, at, say, the gaseous mass' equilibrium rate, the latter's mean rotation may lag/lead the coordinate system's. Material points will then appear to diverge from their equilibrium locations that will be identified as instability, which, although mathematically correct, is physically unreasonable. This may happen even if the rotating frame moves with the body's inertia ellipsoid's principal axes; recall the case of Dedekind ellipsoids. A body's mean rotation is linked to the rigid rotation embedded in its motion, which needs to be isolated, and then ignored, by the coordinate system during a stability analysis.

One way to locate such an appropriate coordinate system $\mathscr{O}$ is to express in it the body's total angular momentum about its mass centre:

$$\boldsymbol{H} = \int_V \boldsymbol{x} \times \rho \left(\boldsymbol{v} + \boldsymbol{\omega} \times \boldsymbol{x}\right) \mathrm{d}V = \boldsymbol{H}_{rel} + \int_V \boldsymbol{x} \times \left(\boldsymbol{\omega} \times \boldsymbol{x}\right) \rho \, \mathrm{d}V, \tag{4.1}$$

where $\boldsymbol{\omega}$ is $\mathscr{O}$'s rotation rate, and we have introduced

$$\boldsymbol{H}_{rel} = \int_V \boldsymbol{x} \times \rho \boldsymbol{v} \, \mathrm{d}V \tag{4.2}$$

as the relative angular momentum observed in $\mathscr{O}$. Expanding the triple product in $\boldsymbol{H}$'s expression, we find that

$$\boldsymbol{H} = \boldsymbol{H}_{rel} + \boldsymbol{J} \cdot \boldsymbol{\omega}. \tag{4.3}$$

where

$$\boldsymbol{J} = \int_V \left(|\boldsymbol{x}|^2 \mathbf{1} - \boldsymbol{x} \otimes \boldsymbol{x}\right) \rho \, \mathrm{d}V = \mathrm{tr}\, \boldsymbol{I} - \boldsymbol{I}. \tag{4.4}$$

is the Euler's moment of inertia tensor. The body's total angular momentum is thus a sum of its relative angular momentum observed in a frame $\mathscr{O}$ rotating at $\boldsymbol{\omega}$ and the

angular momentum the body would have were it rigidly attached to $\mathscr{O}$. It is always possible to locate a coordinate system in which $\boldsymbol{H}_{rel}$ vanishes; these are the Tisserand's mean axes of body (Munk & MacDonald 1960, p. 10). In fact, Tisserand's mean axes minimize the difference $\int_V |\boldsymbol{u} - \boldsymbol{\omega} \times \boldsymbol{x}|^2 \rho \, \mathrm{d}V$ between the actual velocity $\boldsymbol{u}$ of a material point and the velocity that it would have were the body rigid and rotating at $\boldsymbol{\omega}$. Thus, the Tisserand's mean axes of body appear to best isolate the mean rigid rotation within a body's motion and they, therefore, define an appropriate frame $\mathscr{O}$ in which to investigate stability of a freely rotating system. We now see how $\mathscr{O}$'s rotation rate changes.

We investigate the system's stability by providing an initial velocity perturbation $\boldsymbol{v}_o$ and then following its subsequent growth/decay. Such perturbations may abruptly change the system's angular momentum $\boldsymbol{H}$. Therefore, because the frame $\mathscr{O}$ maintains $\boldsymbol{H}_{rel}$ at zero, its rotation rate may change instantaneously from $\boldsymbol{\omega}_E$ just before perturbation ($t = 0^-$) to, say, $\boldsymbol{\omega}_0$ immediately after ($t = 0^+$). We anticipate future application to the rotating ellipsoids of § 3, and identify $\mathscr{O}$'s angular velocity at $t = 0^-$ with their equilibrium rate $\boldsymbol{\omega}_E$. We now relate $\boldsymbol{\omega}_0$ and $\boldsymbol{\omega}_E$.

The velocity field $\boldsymbol{v}_o$ may be perceived in two different ways, namely, as $\boldsymbol{v}_o$ in $\mathscr{O}$ at $t = 0^-$, and as $\boldsymbol{v}_0$ in $\mathscr{O}$ at $t = 0^+$. Let

$$\boldsymbol{H}_p = \int_V \boldsymbol{x} \times \boldsymbol{v}_o \rho \, \mathrm{d}V \tag{4.5}$$

be the angular momentum introduced by the velocity perturbation, so that $\boldsymbol{H}|_{t=0^+} = \boldsymbol{H}_p + \boldsymbol{H}|_{t=0^-}$. Because $\boldsymbol{H}_{rel}|_{t=0-} = \boldsymbol{H}_{rel}|_{t=0^+} = 0$, (4.3) suggests that

$$\boldsymbol{J} \cdot \boldsymbol{\omega}_0 = \boldsymbol{H}_p + \boldsymbol{J} \cdot \boldsymbol{\omega}_E, \tag{4.6}$$

so that

$$\boldsymbol{\omega}_0 = \boldsymbol{\omega}_E + \boldsymbol{J}^{-1} \cdot \boldsymbol{H}_p. \tag{4.7}$$

Therefore, unless the velocity perturbations introduce no angular momentum, the frame $\mathscr{O}$'s rotation rate will jump, while if $\boldsymbol{H}_p = 0$, $\boldsymbol{\omega}_0 = \boldsymbol{\omega}_E$. It will also be necessary to relate $\boldsymbol{v}_0$ to $\boldsymbol{\omega}_E$ and $\boldsymbol{v}_o$. From the definitions of $\boldsymbol{v}_o$, $\boldsymbol{v}_0$, $\boldsymbol{\omega}_E$ and $\boldsymbol{\omega}_0$ it follows that

$$\boldsymbol{v}_0(\boldsymbol{x}, t) = \boldsymbol{v}_o(\boldsymbol{x}, t) - (\boldsymbol{\omega}_0 - \boldsymbol{\omega}_E) \times \boldsymbol{x} = \boldsymbol{v}_o(\boldsymbol{x}, t) - \left(\boldsymbol{J}^{-1} \cdot \boldsymbol{H}_p\right) \times \boldsymbol{x}. \tag{4.8}$$

Again, if $\boldsymbol{H}_p$ vanishes, $\boldsymbol{v}_0$ equals $\boldsymbol{v}_o$.

Finally, post-perturbation $\boldsymbol{H}_{rel}$ remains zero. The total angular momentum $\boldsymbol{H}$ of a free body also remains constant. Thus, taking the time derivative of (4.3) with respect to an observer in $\mathscr{O}$, we must have

$$\dot{\boldsymbol{H}} = -\boldsymbol{\omega} \times \boldsymbol{H} = \frac{\mathrm{d}}{\mathrm{d}t} (\boldsymbol{J} \cdot \boldsymbol{\omega}) = \dot{\boldsymbol{J}} \cdot \boldsymbol{\omega} + \boldsymbol{J} \cdot \dot{\boldsymbol{\omega}}, \tag{4.9}$$

so that, after replacing for $\boldsymbol{H}$ from (4.3), we find

$$\dot{\boldsymbol{\omega}} = -\boldsymbol{J}^{-1} \cdot \left\{ \boldsymbol{\omega} \times (\boldsymbol{J} \cdot \boldsymbol{\omega}) + \dot{\boldsymbol{J}} \cdot \boldsymbol{\omega} \right\}. \tag{4.10}$$

This is the rate at which $\mathscr{O}$'s $\boldsymbol{\omega}$ must change during the perturbed motion so that the body's angular momentum relative to $\mathscr{O}$ is preserved. Specializing to bodies that post-perturbation rotate about a principal axes of inertia, we obtain

$$\dot{\boldsymbol{\omega}} = -\boldsymbol{J}^{-1} \cdot \dot{\boldsymbol{J}} \cdot \boldsymbol{\omega}. \tag{4.11}$$

For homogeneously deforming ellipsoids, $\dot{\boldsymbol{J}}$ is obtained by differentiating (4.4) and employing (2.15):

$$\dot{\boldsymbol{J}} = \mathrm{tr}(\boldsymbol{L}\cdot\boldsymbol{I} + \boldsymbol{I}\cdot\boldsymbol{L}^{\mathrm{T}})\,\mathbf{1} - \left(\boldsymbol{L}\cdot\boldsymbol{I} + \boldsymbol{I}\cdot\boldsymbol{L}^{\mathrm{T}}\right). \tag{4.12}$$

4.2. *The energy criterion*

In the past, Hill (1957), Chakrabarty (1969) and Storåkers (1977) have put forward increasingly generalized versions of the energy criterion for non-smooth rigid-plastic materials, with the last author also addressing systems that rotate, albeit at a constant rate. We extend the energy criterion to freely rotating non-smooth systems. The stability criterion so derived subsumes as special cases results of the works cited above.

The equilibrated body is perturbed at time $t = 0$ by an initial velocity field $\boldsymbol{v}(\boldsymbol{x}, 0) = \boldsymbol{v}_o(\boldsymbol{x})$ field relative to the rotating frame $\mathscr{O}$ that rotated at $\boldsymbol{\omega}_E$ up until $t = 0^-$. As discussed in § 4.1, $\mathscr{O}$'s rotation rate will change to $\boldsymbol{\omega}_0$ at $t = 0^+$ to keep $\boldsymbol{H}_{rel}$ zero; see (4.7). Thus, relative to $\mathscr{O}$ at $t = 0^+$, the body's material points will appear to have an initial velocity $\boldsymbol{v}_0(\boldsymbol{x})$; see (4.8). Subsequently, over the small time δt, these material points will displace by $\int_0^{\delta t} \boldsymbol{v}\,\mathrm{d}t$. The work done by external agencies during δt is

$$\delta W = \int_0^{\delta t}\int_{V(t)} \rho\,\boldsymbol{b}_R\cdot\boldsymbol{v}\,\mathrm{d}V\,\mathrm{d}t + \int_0^{\delta t}\int_{S(t)} \boldsymbol{N}\cdot\boldsymbol{v}\,\mathrm{d}S\,\mathrm{d}t = \int_0^{\delta t}\int_{V(t)} \rho\,\boldsymbol{b}_R\cdot\boldsymbol{v}\,\mathrm{d}V\,\mathrm{d}t, \tag{4.13}$$

as the surface forces $\boldsymbol{N}$ are absent in the current problem and $\boldsymbol{b}_R = \boldsymbol{b} - \dot{\boldsymbol{\Omega}}\cdot\boldsymbol{x} - \boldsymbol{\Omega}^2\cdot\boldsymbol{x} - 2\boldsymbol{\Omega}\cdot\boldsymbol{v}$ is the apparent body force experienced in the rotating frame $\mathscr{O}$. Meanwhile, the energy stored/dissipated over δt is

$$\delta E = \int_0^{\delta t}\int_{V(t)} \boldsymbol{\sigma} : \boldsymbol{L}\,\mathrm{d}V\,\mathrm{d}t. \tag{4.14}$$

Everywhere above, the integration is over the body's possibly changing current volume.

Stability is ensured by the energy criterion if $\delta E > \delta W$. This inequality may be alternatively viewed by taking dot product of (2.2) with the velocity v and integrating first over the volume and then in time from 0 to δt, to find that

$$\delta W - \delta E = \int_0^{\delta t}\int_{V(t)} \rho\frac{\mathrm{d}}{\mathrm{d}t}\left(\frac{v^2}{2}\right)\mathrm{d}V\,\mathrm{d}t = \delta E_k, \tag{4.15}$$

the change in the relative kinetic energy observed in the frame $\mathscr{O}$. The energy criterion guarantees stability in $\mathscr{O}$ if the relative kinetic energy's increment is negative, i.e.

$$\delta E_k < 0. \tag{4.16}$$

Employing earlier estimates for δE and δW, and replacing for $\boldsymbol{b}_R$ provides

$$\delta E_k = \int_0^{\delta t}\int_{V(t)} \rho\left(\boldsymbol{b} - \boldsymbol{\Omega}^2\cdot\boldsymbol{x} - \dot{\boldsymbol{\Omega}}\cdot\boldsymbol{x}\right)\cdot\boldsymbol{v}\,\mathrm{d}V\,\mathrm{d}t - \int_0^{\delta t}\int_{V(t)} \boldsymbol{\sigma} : \boldsymbol{L}\,\mathrm{d}V\,\mathrm{d}t, \tag{4.17}$$

where the Coriolis' force term has dropped out because $(2\boldsymbol{\Omega}\cdot\boldsymbol{v})\cdot\boldsymbol{v} = (2\boldsymbol{\omega}\times\boldsymbol{v})\cdot\boldsymbol{v} \equiv 0$. The Coriolis' force, which is gyroscopic in nature, does not do any work, and so is overlooked by the energy criterion.

Examining (4.16) is not straightforward, as the integrals in δE_k's expression are not easily resolved. Within the confines of a local stability analysis, the inequality (4.16) needs to be tested only for small displacements following a velocity perturbation, i.e. over small time δt. This prompts the expansion

$$\delta E_k = \delta^{(1)}E_k \delta t + \delta^{(2)}E_k \tfrac{1}{2}\delta t^2 + \cdots. \tag{4.18}$$

According to the energy criterion, the system is locally stable if the first non-zero term in the above expansion is negative. Here we restrict ourselves to checking only the first two terms. To facilitate a δE_k's series expansion, we interchange the orders of temporal and spatial integration by converting the domain of spatial integration from the time-dependent current volume to the fixed initial unperturbed volume V_0:

$$\delta E_k = \int_{V_0}\int_0^{\delta t} \rho_0 \left(\boldsymbol{b} - \boldsymbol{\Omega}^2\cdot\boldsymbol{x} - \dot{\boldsymbol{\Omega}}\cdot\boldsymbol{x}\right)\cdot\boldsymbol{v}\,\mathrm{d}t\,\mathrm{d}V_0 - \int_{V_0}\int_0^{\delta t} \boldsymbol{\sigma} : \boldsymbol{L}\boldsymbol{J}^{-1}\,\mathrm{d}t\,\mathrm{d}V_0 \tag{4.19}$$

where ρ_0 is the density at equilibrium and $J = \rho/\rho_0 = \mathrm{d}V_0/\,\mathrm{d}V$ is the Jacobian relating the current and equilibrium volumes. Expressions for the ith-order estimate $\delta^{(i)}E_k$ are found by expanding various fields above in a Taylor series about $t = 0^+$. We obtain

$$\delta^{(1)}E_k = -\int_{V_0}\left[\boldsymbol{\sigma}_0 : \boldsymbol{L}_0 - \left(\rho_0\boldsymbol{b}_0 - \boldsymbol{\Omega}_0^2\cdot\boldsymbol{x}_0 - \dot{\boldsymbol{\Omega}}_0\cdot\boldsymbol{x}_0\right)\cdot\boldsymbol{v}_0\right]\mathrm{d}V_0 \tag{4.20a}$$

and

$$\begin{aligned}\delta^{(2)}E_k = \int_{V_0}\big[&-\dot{\boldsymbol{\sigma}}_0 : \boldsymbol{L}_0 - \boldsymbol{\sigma}_0 : \dot{\boldsymbol{L}}_0 + \boldsymbol{\sigma}_0 : \boldsymbol{L}_0\dot{J}_0 + \rho_0\big\{\dot{\boldsymbol{b}}_0 - \boldsymbol{\Omega}_0^2\cdot\boldsymbol{v}_0 \ \ldots\\ &\cdots - \left(\dot{\boldsymbol{\Omega}}_0\cdot\boldsymbol{\Omega}_0 + \boldsymbol{\Omega}_0\cdot\dot{\boldsymbol{\Omega}}_0 + \ddot{\boldsymbol{\Omega}}_0\right)\cdot\boldsymbol{x}_0\big\}\cdot\boldsymbol{v}_0 + \rho_0\left(\boldsymbol{b}_0 - \boldsymbol{\Omega}_0^2\cdot\boldsymbol{x}_0 - \dot{\boldsymbol{\Omega}}_0\cdot\boldsymbol{x}\right)\cdot\dot{\boldsymbol{v}}_0\big]\,\mathrm{d}V_0,\end{aligned} \tag{4.20b}$$

where the subscript '0' indicates evaluation at $t = 0^+$, so that $J_0 = 1$ and $\ddot{\boldsymbol{\Omega}}_0$ is the antisymmetric tensor corresponding to $\ddot{\boldsymbol{\omega}}_0$. A velocity perturbation cannot instantaneously change a material point's location $\boldsymbol{x}$ or fields that depend only on $\boldsymbol{x}$, so that accompanying subscripts are henceforth dropped. In contrast, $\mathscr{O}$'s rotation rate, see (4.7), and the stress field – see figure 2's caption – may change suddenly, and we introduce the jumps:

$$\Delta\boldsymbol{\omega} = \boldsymbol{\omega}_0 - \boldsymbol{\omega}_E = \boldsymbol{J}^{-1}\cdot\boldsymbol{H}_p \quad \text{and} \quad \Delta\boldsymbol{\sigma} = \boldsymbol{\sigma}_0 - \boldsymbol{\sigma}_E. \tag{4.21}$$

For small δt, δE_k's sign is the same as $\delta^{(1)}E_k$'s, so that local stability is guaranteed if

$$\delta^{(1)}E_k < 0. \tag{4.22}$$

Replacing from (4.21) and recognizing power balance at equilibrium, we find that

$$\delta^{(1)}E_k = -\int_V \left[\Delta\boldsymbol{\sigma} : \boldsymbol{L}_0 + \boldsymbol{x}\cdot\left(\Delta\boldsymbol{\Omega}^2 + \Delta\boldsymbol{\Omega}\cdot\boldsymbol{\Omega}_E + \boldsymbol{\Omega}_E\cdot\Delta\boldsymbol{\Omega} - \dot{\boldsymbol{\Omega}}_0\right)\cdot\boldsymbol{v}_0\right]\mathrm{d}V, \tag{4.23}$$

where $\Delta\boldsymbol{\Omega}$ is the angular velocity tensor corresponding to the jump $\Delta\boldsymbol{\omega}$ in $\boldsymbol{\omega}$. The estimate $\delta^{(1)}E_k$ vanishes identically if the perturbations are such that: (*a*) the stress jump accompanying the applied perturbation do not input any power; (*b*) no relative angular momentum $\boldsymbol{H}_p$ is introduced, so that $\Delta\boldsymbol{\Omega} = 0$; and (*c*) the contribution $\int_V \boldsymbol{x}\cdot\dot{\boldsymbol{\Omega}}_0\cdot\boldsymbol{v}_0\,\mathrm{d}V$ from the frame $\mathscr{O}$'s post-perturbation angular acceleration $\dot{\boldsymbol{\omega}}_0$ vanishes.

For those $\boldsymbol{v}_0$ for which $\delta^{(1)}E_k$ vanishes, the energy criterion requires that for stability

$$\delta^{(2)}E_k < 0. \tag{4.24}$$

With $\dot{J}\big|_{t=0} = \mathrm{tr}(\boldsymbol{L}_0)$, and setting $\boldsymbol{\Omega}_0 = \boldsymbol{\Omega}_E$ when $\boldsymbol{H}_p = 0$, $\delta^{(2)}E_k$ becomes

$$\delta^{(2)}E_k = \int_V \big[\{\boldsymbol{\sigma}_0 \mathrm{tr}(\boldsymbol{L}_0) \; - \dot{\boldsymbol{\sigma}}_0\} : \boldsymbol{L}_0 - \boldsymbol{\sigma}_0 : \dot{\boldsymbol{L}}_0 + \rho \left\{\dot{\boldsymbol{b}}_0 - \boldsymbol{\Omega}_E^2 \cdot \boldsymbol{v}_0 \ldots \right. \\ \left. \cdots - \left(\dot{\boldsymbol{\Omega}}_0 \cdot \boldsymbol{\Omega}_E + \boldsymbol{\Omega}_E \cdot \dot{\boldsymbol{\Omega}}_0 + \ddot{\boldsymbol{\Omega}}_0\right) \cdot \boldsymbol{x}\right\} \cdot \boldsymbol{v}_0 + \rho \left(\boldsymbol{b}_0 - \boldsymbol{\Omega}_E^2 \cdot \boldsymbol{x} - \dot{\boldsymbol{\Omega}}_0 \cdot \boldsymbol{x}\right) \cdot \dot{\boldsymbol{v}}_0\big] \, \mathrm{d}V. \tag{4.25}$$

Once an appropriate constitute law is selected, satisfaction of the inequality (4.22) or (4.24), as the case may be, with $\delta^{(1)}E_k$ and $\delta^{(2)}E_k$ given as above, for all kinematically admissible velocity perturbations ensures local stability, and may be employed to check the stability of any continuous system. It is practically impossible to check the inequality (4.22) or (4.24) for all possible admissible fields. Thus, often, a stability investigation is restricted to velocity perturbations belonging to a functional class, e.g., the homogeneous deformations introduced previously. This we now do.

4.3. *Homogeneous modes*

We specialize the energy criterion to investigate the stability of self-gravitating incompressible homogeneously deforming fluid and Bingham fluid ellipsoids freely rotating about their axis of maximum inertia $\hat{\boldsymbol{e}}_3$. The equilibria of such ellipsoids were explored earlier. We restrict ourselves to incompressible perturbations of the kind

$$\boldsymbol{v}_o = \boldsymbol{D}_o \cdot \boldsymbol{x} \tag{4.26}$$

with $\mathrm{tr}(\boldsymbol{D}_o) = 0$; these perturbations when observed in the frame $\mathscr{O}$ at $t = 0^-$ do not carry any material spin. Nevertheless, (4.5) suggests that these perturbations introduce the angular momentum

$$\boldsymbol{H}_p = -2\mathrm{ax}\,\mathrm{sk}(\boldsymbol{I} \cdot \boldsymbol{D}_o), \tag{4.27}$$

where $\mathrm{sk}(\boldsymbol{B})$ returns a tensor $\boldsymbol{B}$'s antisymmetric part, while $\mathrm{ax}\,\mathrm{sk}(\boldsymbol{B})$ is the corresponding axial vector. Thus, (4.7) suggests that $\mathscr{O}$'s rotation rate $\boldsymbol{\omega}$ changes abruptly and from (4.8),

$$\boldsymbol{v}_0 = \left(\boldsymbol{D}_o - \boldsymbol{J}^{-1} \cdot \boldsymbol{H}_p\right) \cdot \boldsymbol{x} =: \boldsymbol{L}_0 \cdot \boldsymbol{x} \tag{4.28}$$

will be the observed velocity perturbation in $\mathscr{O}$ at $t = 0^+$ and $\boldsymbol{L}_0$ the corresponding velocity gradient. Now δE_k's first-order estimate $\delta^{(1)}E_k$ developed earlier simplifies to

$$\delta^{(1)}E_k = -\left\{\Delta\overline{\boldsymbol{\sigma}}_0 V + \boldsymbol{I} \cdot \left(\Delta\boldsymbol{\Omega}^2 + \boldsymbol{\Omega}_E \cdot \Delta\boldsymbol{\Omega} + \Delta\boldsymbol{\Omega} \cdot \boldsymbol{\Omega}_E - \dot{\boldsymbol{\Omega}}_0\right)\right\} : \boldsymbol{L}_0. \tag{4.29}$$

We will have reason to investigate stability at second order only when $\delta^{(1)}E_k$ vanishes, the conditions for which were noted earlier. We probe them assuming homogeneous dynamics.

Perturbations add angular momentum $\boldsymbol{H}_p$ given by (4.27) unless $\boldsymbol{I}$ and $\boldsymbol{D}_o$ commute. When $\boldsymbol{H}_p = 0$, $\Delta\boldsymbol{\omega} = 0$, so that

$$\boldsymbol{\omega}_0 = \boldsymbol{\omega}_E, \quad \boldsymbol{L}_0 = \boldsymbol{D}_o \quad \text{and} \quad \boldsymbol{v}_0 = \boldsymbol{v}_o = \boldsymbol{D}_o \cdot \boldsymbol{x}. \tag{4.30}$$

Finally, from (4.11), we observe that immediately after the perturbation the frame $\mathscr{O}$'s angular acceleration $\dot{\boldsymbol{\omega}}_0$ does not in general vanish. Its contribution to $\delta^{(1)}E_k$ is found to be proportional to $\mathrm{tr}(\dot{\boldsymbol{\Omega}} \cdot \boldsymbol{I} \cdot \boldsymbol{L}^{\mathrm{T}})\big|_0$ after replacing (4.28) in $\delta^{(1)}E_k$'s expression above. This contribution vanishes with $\boldsymbol{H}_p$. Thus, when $\boldsymbol{H}_p$ is absent, not only does $\mathscr{O}$'s rotation rate not jump, its angular acceleration does not affect stability at $O(\delta t)$.

Similarly, stress may change suddenly across a perturbation; cf. the caption to figure 2. In incompressible inviscid fluids this is due to a sudden jump in pressure. Indeed, in incompressible self-gravitating Bingham fluid ellipsoids restricted to homogeneous dynamics, the average non-dimensional pressure $\overline{p}$ may be obtained by taking the trace of dynamical equations (2.14) and employing (2.12):

$$\overline{p} = \frac{1}{V}\frac{2 + \operatorname{tr}(\boldsymbol{L}^2 + \boldsymbol{\Omega}^2 + 2\boldsymbol{\Omega}\cdot\boldsymbol{L})}{3\operatorname{tr}(\boldsymbol{I}^{-1})} + Y\frac{\operatorname{tr}(\boldsymbol{D}\cdot\boldsymbol{I}^{-1})}{3\,|\boldsymbol{D}|\,\operatorname{tr}(\boldsymbol{I}^{-1})}. \tag{4.31}$$

Note that we recover the case of inviscid fluids when $Y = 0$. Thus, the average pressure in incompressible fluids changes from its equilibrium value $\overline{p}_E$ to $\overline{p}_0$ instantly following a velocity perturbation, and we define its jump by

$$\Delta p = \overline{p}_0 - \overline{p}_E. \tag{4.32}$$

In Bingham fluids, the stress state may also shift suddenly if incompatible perturbations are imposed, see figure 2, and we discuss this in a later section.

Perturbations for which both $\boldsymbol{H}_p$ and $\Delta\boldsymbol{\sigma}$'s power input are zero, $\delta^{(1)}E_k$ vanishes, and δE_k's sign for small δt is regulated by $\delta^{(2)}E_k$. To simplify $\delta^{(2)}E_k$'s expression given previously we need to evaluate $\dot{\boldsymbol{b}}$ and $\dot{\boldsymbol{v}}_0$. Employing (2.8) for body force within self-gravitating bodies, utilizing the second of (4.30), and scaling time by $1/\sqrt{2\pi\rho G}$ as usual, we find

$$\dot{\boldsymbol{b}}_0 = -\dot{\boldsymbol{A}}_0\cdot\boldsymbol{x} - \boldsymbol{A}\cdot\boldsymbol{v}_0 = -\left(\dot{\boldsymbol{A}}_0 + \boldsymbol{A}\cdot\boldsymbol{D}_o\right)\cdot\boldsymbol{x}. \tag{4.33}$$

Differentiating (4.28) and employing the second of (4.30), we obtain

$$\dot{\boldsymbol{v}}_0 = \left(\dot{\boldsymbol{L}}_0 + \boldsymbol{D}_o^2\right)\cdot\boldsymbol{x}. \tag{4.34}$$

Substituting the above formulae in $\delta^{(2)}E_k$, utilizing (4.30) and incompressibility yields

$$\begin{aligned}\delta^{(2)}E_k = &-\left(\dot{\boldsymbol{A}}_0 + 4\boldsymbol{\Omega}_E\cdot\dot{\boldsymbol{\Omega}}_0\right)\cdot\boldsymbol{I} : \boldsymbol{D}_o + \overline{\boldsymbol{\sigma}}_E : \boldsymbol{D}_o^2 V \ldots \\ &\cdots - \overline{\boldsymbol{\sigma}}_E\cdot\Delta\boldsymbol{\sigma} : \boldsymbol{I}^{-1}V^2 - \dot{\overline{\boldsymbol{\sigma}}}_0 : \boldsymbol{D}_o V - \overline{\boldsymbol{\sigma}}_0 : \dot{\boldsymbol{L}}_0 V - \dot{\boldsymbol{\Omega}}_0^2 : \boldsymbol{I},\end{aligned} \tag{4.35}$$

where $\dot{\boldsymbol{\Omega}}_0$ is found from $\dot{\boldsymbol{\omega}}_0$ obtained by combining (4.11) and (4.12). Computing $\dot{\boldsymbol{A}}_0$ is complicated and is done in appendix A. The stress post-perturbation $\overline{\boldsymbol{\sigma}}_0$ is obtained from a constitutive law. In deriving the above form, we utilized (3.1) and the facts that, because $\boldsymbol{\omega}_E$ is along $\hat{\boldsymbol{e}}_3$ and $\boldsymbol{H}_p = 0$, $\boldsymbol{I}$, $\boldsymbol{D}_o$ and $\boldsymbol{\Omega}_E^2$ commute, as also do $\ddot{\boldsymbol{\Omega}}_0$, $\dot{\boldsymbol{\Omega}}_0$ and $\boldsymbol{\Omega}_E$.

For stability to homogeneous perturbations either (4.22) holds with $\delta^{(1)}E_k$ given by (4.29) or, when $\delta^{(1)}E_k = 0$, (4.24) with $\delta^{(2)}E_k$ from (4.35) is true. We next consider two applications.

5. Application

5.1. *Inviscid incompressible fluids*

In such fluids $\overline{\boldsymbol{\sigma}} = -\overline{p}\mathbf{1}$, so that $\Delta\boldsymbol{\sigma} = -\Delta p\mathbf{1}$ and $\dot{\overline{\boldsymbol{\sigma}}}_0 = -\dot{\overline{p}}_0\mathbf{1}$. Stability at first order is checked by evaluating $\delta^{(1)}E_k$. Replacing $\overline{\boldsymbol{\sigma}}$ in (4.29) and recalling that because the fluid is incompressible, velocity perturbations must be such that $\operatorname{tr}(\boldsymbol{L}_0) = 0$, we obtain

$$\delta^{(1)}E_k = -\boldsymbol{I}\cdot\left(\Delta\boldsymbol{\Omega}^2 + \boldsymbol{\Omega}_E\cdot\Delta\boldsymbol{\Omega} + \Delta\boldsymbol{\Omega}\cdot\boldsymbol{\Omega}_E - \dot{\boldsymbol{\Omega}}_0\right) : \boldsymbol{L}_0; \tag{5.1}$$

note that pressure jump Δp, although present, does not play any role. When the perturbations are such that $\delta^{(1)}E_k$ equals zero, we evaluate $\delta^{(2)}E_k$. Replacing in (4.35)

for $\overline{\boldsymbol{\sigma}}_0$ and setting $\mathrm{tr}(\boldsymbol{D}_o) = \mathrm{tr}(\dot{\boldsymbol{L}}_0) = 0$, we find

$$\delta^{(2)}E_k = -\left(\dot{\boldsymbol{A}}_0 + 4\boldsymbol{\Omega}_E \cdot \dot{\boldsymbol{\Omega}}_0\right) \cdot \boldsymbol{I} : \boldsymbol{D}_o - \overline{p}_E \mathrm{tr}(\boldsymbol{D}_o^2)\, V - \Delta p \overline{p}_E \mathrm{tr}(\boldsymbol{I}^{-1})\, V^2 - \dot{\boldsymbol{\Omega}}_0^2 : \boldsymbol{I}. \quad (5.2)$$

We now consider the stability of the Maclaurin and Jacobi ellipsoids in turn.

5.1.1. *Maclaurin spheroids*

Maclaurin spheroids are identified by $a_1 = a_2 \geqslant a_3$, so that $I_1 = I_2$ and only perturbations with non-zero D_{23} and/or D_{31} introduce angular momentum $\boldsymbol{H}_p$. Investigating perturbations with $D_{12} \neq 0$ is unnecessary, as the axial symmetry of the Maclaurin spheroids always allows selecting a coordinate system that is aligned at equilibrium to ensure that D_{12} is zero. If $\boldsymbol{H}_p \neq 0$, it is possible to find perturbations that will make $\delta^{(1)}E_k > 0$, so that Maclaurin spheroids are secularly unstable. Indeed, selecting $D_{11} = -D_{22}$ and all other strain rates except D_{23} to be zero, we find that

$$\delta^{(1)}E_k = -\frac{(I_3 - I_1)^2 I_1}{(I_3 + I_1)^2} D_{23}^2 D_{11}, \quad (5.3)$$

which may be made positive or negative by appropriately selecting D_{11}.

Restricting to perturbations for which $\boldsymbol{H}_p = 0$, because $\delta^{(1)}E_k$ vanishes, we need to consider $\delta^{(2)}E_k$. Replacing for $\boldsymbol{A}$, $\dot{\boldsymbol{A}}_0$, $\boldsymbol{\Omega}_E$, $\dot{\boldsymbol{\Omega}}_0$ and p_E from, respectively, (2.9), (A 10), (3.11), (4.11) and (3.3), evaluating Δp from (4.32), (3.1) and (4.31) evaluated at $t = 0^+$, and setting $a_3 = a_1\beta$, we obtain

$$\begin{aligned}\frac{5}{ma_1^2}\delta^{(2)}E_k = &\left\{2\left(A_{1_\alpha} - A_{2_\alpha}\right) + \left(A_{1_\beta} - A_{2_\beta}\right)\beta - 4\beta^2 A_3\right\} D_{11}^2 \ldots \\ &\cdots + \left\{\left(A_{1_\alpha} - 3A_{2_\alpha} + 2\beta^2 A_{3_\alpha}\right) - \left(A_{1_\beta} - \beta^2 A_{3_\beta}\right)\beta - 4\beta^2 A_3\right\} D_{11} D_{33} \ldots \\ &\cdots - \left\{\left(A_{2_\alpha} - \beta^2 A_{3_\alpha}\right) - \left(A_{2_\beta} - \beta^2 A_{3_\beta}\right)\beta + 2\left(A_1 + \beta^2 A_3\right)\right\} D_{33}^2, \quad (5.4)\end{aligned}$$

where $A_{i\alpha}$ and $A_{i\beta}$ are, respectively, $\partial A_i/\partial\alpha$ and $\partial A_i/\partial\beta$ found for oblate ellipsoids in (A 7*a*). The right-hand side above is a quadratic form in terms of the vector $\boldsymbol{d} = \{D_{11}, D_{33}\}$ and may be expressed as $d_m q_{mn} d_n$. Thus, stability will be ensured if the eigenvalues of the 2×2 matrix q_{mn} are all negative. These we compute numerically. We find that for $\beta < \beta_J = 0.587$, the eigenvalue corresponding to the perturbation $D_{11} = -D_{22}$ becomes positive. Chandrasekhar (1969) identified this mode as the toroidal mode. Thus, the energy criteria assures us that all Maclaurin spheroids with axes ratio $\beta \geqslant \beta_J$, i.e., beyond the point from which the Jacobi ellipsoids bifurcate, are secularly stable.

Consider stability predictions for perturbations that preserve angular momentum. Chandrasekhar (1969) found by his spectral method that the Maclaurin spheroid was neutrally unstable at $\beta = \beta_J$, i.e., one eigenmode's oscillation frequency vanished, and ordinarily unstable for $\beta < \beta_R = 0.3033$ where a Riemann sequence bifurcates from the Maclaurin spheroids. For $\beta_R < \beta < \beta_J$ the Maclaurin spheroids were found to be dynamically stable but secularly unstable; see Rosenkilde (1967). In contrast to Chandrasekhar (1969), our application of the energy method predicts that for β below β_J the Maclaurin ellipsoids are secularly unstable and nothing special is observed at $\beta = \beta_R$. At the same time, Riemann (1860) employing the energy method in the classical sense of form (i), which is equivalent to the present analysis for inviscid fluids, uncovered that Maclaurin spheroids are secularly stable to homogeneous perturbations for all $\beta > \beta_R$. On the other hand, Lyttleton (1953) and

Jeans (1961) also applying the energy criterion in form (i) arrived at the same result as us, i.e., secular stability for $\beta > \beta_J$. Now, our prediction and those of Jeans and Lyttleton are consistent with Chandrasekhar's spectral analysis; Maclaurin ellipsoids with $\beta_R < \beta < \beta_J$ are stabilized by gyroscopic forces whose effects are missed by an energy analysis. However, Riemann's results appear contradictory and need to be reconciled. The answer lies in the manner the system's 'kinetic energy' was defined when applying the energy criterion. While we, and earlier Jeans and Lyttleton, select E_k defined by (4.24) as kinetic energy, Riemann defined the Maclaurin spheroid to be stable as long as the change $\delta \sum \dot{a}_i^2$ was negative post-perturbation; $\sum \dot{a}_i^2$ was thus identified by Riemann as a measure of the system's 'kinetic energy'. This choice was natural for Riemann who followed Dirichlet and phrased the dynamical evolution of a homogeneously deforming ellipsoid in terms of its semi-major axes; see Chandrasekhar (1969, p. 173, equations (236)–(238)). However, there is no reason to believe that a negative change in E_k following a perturbation necessitates a drop in $\sum \dot{a}_i^2$. Indeed, numerical integration of the associated dynamical equations (2.14) confirm this fact. Following a perturbation, $\sum \dot{a}_i^2$ only begins to grow for $\beta < \beta_R$, while E_k increases for all β less than β_J. This is illustrated in figure 6. Riemann was thus checking for the stability of the ellipsoid's shape and not its stability as a material body. It is, therefore, crucial to clearly identify the system's 'kinetic energy' in an energy analysis as different definitions may not be equivalent. In this context, we also mention the recent work of Lai, Rasio & Shapiro (1993) who considered the stability of compressible inviscid fluid ellipsoids. These authors tested stability by minimizing an energy functional that was allowed to depend on parameters such as the ellipsoid's shape, density, mass, angular momentum, and internal vorticity. Equilibriums solutions were distinguished by the presence/absence of internal vorticity. The points of instability at β_R and β_J corresponded to energy minima of these two solution sets, respectively. This is reminiscent of different definitions of kinetic energy that include/exclude vorticity.

5.1.2. *Jacobi ellipsoids*

We now investigate the stability of the truly triaxial Jacobi ellipsoids. Perturbations with non-zero shear rates add angular momentum $\boldsymbol{H}_p$ and $\delta^{(1)}E_k$'s sign is to be tested. As for Maclaurin spheroids, it is possible to find homogeneous perturbations that render $\delta^{(1)}E_k$ positive, so that Jacobi ellipsoids are also secularly unstable if all homogeneous perturbations are permitted. If we restrict perturbations to those for which $\boldsymbol{H}_p$ is zero, these involve only axial strain rates, then $\delta^{(1)}E_k$ vanishes and we consider $\delta^{(2)}E_k$'s sign.

As before, we replace for $\boldsymbol{\Omega}$, and for $\boldsymbol{A}$ and $\dot{\boldsymbol{A}}_0$ in (5.2) to obtain $\delta^{(2)}E_k$ as the quadratic form $d_m q_{mn} d_n$. For stability we require q_{mn}'s eigenvalues to be negative for all axial $\boldsymbol{D}_o$. This is found to be true, so that the Jacobi ellipsoids are stable to all homogeneous perturbations that do not add angular momentum. This is consistent with Chandrasekhar's (1969) spectral results and those of Lyttleton (1953) and Jeans (1961).

When we frame the energy criterion in a coordinate system that rotates at a fixed rate equalling the ellipsoid's equilibrium rate $\boldsymbol{\omega}_E$, we find that even for those perturbations for which $\boldsymbol{H}_p$ is zero, $\delta^{(2)}E_k$ is positive, i.e., the Jacobi ellipsoids are secularly unstable. This has been noted by Jeans (1961) and Lyttleton (1953), and reinforces the importance of appropriately selecting the coordinate system in which to test secular stability.

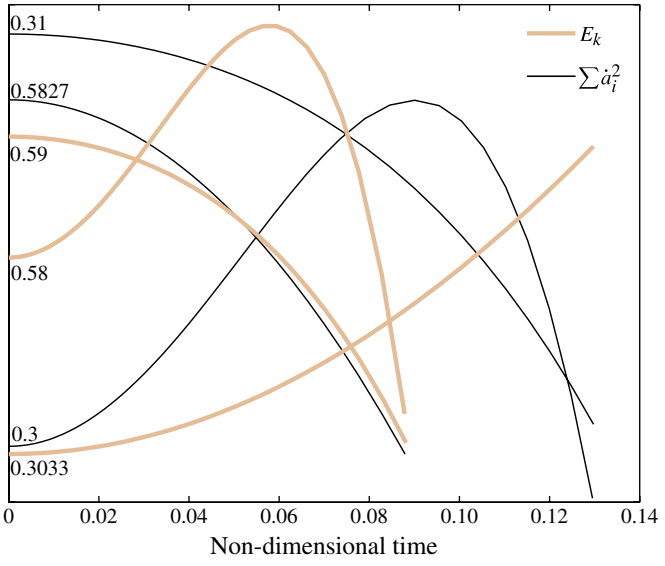

FIGURE 6. (Colour online) Variation of E_k and $\sum \dot{a}_i^2$ with time immediately after perturbation. The numbers next to each curve identify the corresponding axes ratio β at equilibrium.

5.2. *Bingham fluids*

We now apply the energy criterion to investigate the stability of freely rotating self-gravitating Bingham fluid ellipsoids. Owing to its non-smooth constitutive structure, stability may not be tested by the spectral method. For obvious reasons, we will test the stability of only the boundaries of equilibrium regions corresponding to various choices of the yield stress Y. We will subsequently refer to ellipsoids lying on the boundary of the equilibrium region corresponding to their yield stress as critically equilibrated ellipsoids.

Consider first perturbations that impart angular momentum. Checking $\delta^{(1)}E_k$'s sign, we find that, just as in the case of inviscid fluids, it may be positive for some perturbations. Bingham fluid ellipsoids are thus also secularly unstable if we admit homogeneous perturbations for which $\boldsymbol{H}_p \neq 0$.

We now restrict ourselves to perturbations that do not add any angular momentum. We still have to consider the possibility of the stress tensor's jump $\Delta\boldsymbol{\sigma}$ that accompanies an incompatible perturbation contributing to $\delta^{(1)}E_k$. This was not a concern in the case of inviscid incompressible fluids where pressure did no work. In Bingham fluids there is an additional term $Y\boldsymbol{D}_o/|\boldsymbol{D}_o|$ that may contribute non-zero power. Indeed, when $\boldsymbol{H}_p = 0$,

$$\delta^{(1)}E_k = -\Delta\overline{\boldsymbol{\sigma}}_0 V : \boldsymbol{L}_0 = -\left(\overline{\boldsymbol{\sigma}}_0 - \overline{\boldsymbol{\sigma}}_E\right) : \boldsymbol{D}_o V. \tag{5.5}$$

Appealing to figure 2 and the maximum dissipation postulate mentioned in § 3.2, we have $(\overline{\boldsymbol{\sigma}}_0 - \overline{\boldsymbol{\sigma}}_E) : \boldsymbol{D}_o > 0$, unless $\overline{\boldsymbol{\sigma}}_0 - \overline{\boldsymbol{\sigma}}_E = \Delta\boldsymbol{\sigma} = -\Delta p\mathbf{1}$. Thus, except for compatible perturbations for which $\Delta\boldsymbol{\sigma}$ is hydrostatic, $\delta^{(1)}E_k < 0$, and the energy criterion predicts stability at the first order itself for angular momentum preserving perturbations.

It remains, therefore, to only consider compatible perturbations for which $\boldsymbol{H}_p$ also vanishes. For such perturbations, $\delta^{(1)}E_k$ is identically zero, and we need to consider

$\delta^{(2)}E_k$'s sign. To evaluate $\delta^{(2)}E_k$ from (4.35), we first compute $\dot{\overline{\boldsymbol{\sigma}}}_0$ by differentiating (3.8) and replacing $\boldsymbol{s}$ from (3.9):

$$\dot{\overline{\boldsymbol{\sigma}}}_0 = -\dot{\bar{p}}_0 \mathbf{1} + Y \left\{ \frac{\dot{\boldsymbol{D}}_0}{|\boldsymbol{D}_o|} - \frac{\left(\dot{\boldsymbol{D}}_0 : \boldsymbol{D}_o\right) \boldsymbol{D}_o}{|\boldsymbol{D}_o|^3} \right\}, \tag{5.6}$$

so that $\dot{\overline{\boldsymbol{\sigma}}}_0 : \boldsymbol{D}_o = 0$ for incompressible materials. Employing $\boldsymbol{H}_p = 0$ and $\overline{\boldsymbol{\sigma}}_0 = \overline{\boldsymbol{\sigma}}_E + \Delta\boldsymbol{\sigma}$ in (2.14) yields

$$\dot{\boldsymbol{L}}_0 = -\Delta\boldsymbol{\sigma} \cdot \boldsymbol{I}^{-1} V - \left(\boldsymbol{D}_o^2 + \dot{\boldsymbol{\Omega}}_0 + 2\boldsymbol{\Omega}_E \cdot \boldsymbol{D}_o\right). \tag{5.7}$$

Substituting for $\dot{\boldsymbol{L}}_0$ and $\overline{\boldsymbol{\sigma}}_0$ in $\delta^{(2)}E_k$'s formula, setting $\Delta\boldsymbol{\sigma} = -\Delta p \mathbf{1}$ and $\mathrm{tr}(\boldsymbol{\sigma}_E \cdot \boldsymbol{\Omega}_E \cdot \boldsymbol{D}_o) = 0$ for compatible perturbations that do not carry angular momentum, we find, finally

$$\delta^{(2)}E_k = -\left(\dot{\boldsymbol{A}}_0 + 4\boldsymbol{\Omega}_E \cdot \dot{\boldsymbol{\Omega}}_0\right) \cdot \boldsymbol{I} : \boldsymbol{D}_o + 2\overline{\boldsymbol{\sigma}}_E : \boldsymbol{D}_o^2 V - \dot{\boldsymbol{\Omega}}_0^2 : \boldsymbol{I}, \tag{5.8}$$

with $\dot{\boldsymbol{A}}_0$ available from appendix A, $\boldsymbol{\Omega}_E$ from (3.11), and $\dot{\boldsymbol{\Omega}}_0$ is $\dot{\boldsymbol{\omega}}_0$'s associated antisymmetric tensor obtained in turn from (4.11). Now $\delta^{(2)}E_k$'s sign is to be tested only for compatible perturbations for which $\boldsymbol{H}_p = 0$. Compatible perturbations follow (3.10), i.e.,

$$\frac{D_{11}}{\sigma_{11} + p} = \frac{D_{22}}{\sigma_{22} + p} = \frac{D_{33}}{\sigma_{33} + p}, \tag{5.9}$$

with $D_{ij} = 0$ if $i \neq j$, and σ_{ij} and p_E available from, respectively, (3.1) and (3.3). There is, thus, only one compatible perturbation, and it automatically preserves angular momentum. We need test $\delta^{(2)}E_k$'s sign for this perturbation only.

Consider first oblate ellipsoids. We set $a_1 = a_2$ in (5.8), and evaluate $\delta^{(2)}E_k$ for $0 \leqslant \beta \leqslant 1$ and various choices of yield stress Y. We find that except for critically equilibrated ellipsoids that lie within a small region in shape-spin space comprising of slowly rotating flattened ellipsoids, all other ellipsoids are stable to perturbations of the type (5.9); see figure 7. We note that the stability boundary does not pass through $\beta = \beta_J$ when $Y = 0$, i.e., the point where inviscid fluid ellipsoids become unstable. This is because stability of fluid ellipsoids was decided at second-order by testing all perturbations that did not contribute any angular momentum $\boldsymbol{H}_p$. In contrast, Bingham fluids were found stable at first-order to these very perturbations excepting the compatible perturbation (5.9). This latter perturbation, however, is not the toroidal mode found to be most unstable for inviscid fluid ellipsoids.

Figure 8 shows that, again, except for a small region encompassing very slender slowly rotating critically equilibrated ellipsoids, other prolate Bingham fluid ellipsoids are stable. Finally, in triaxial ellipsoids with $\alpha = (1 + \beta)/2$, we observe that the unstable region expands as a narrow finger and approaches the Jacobi ellipsoid; see figure 9.

We observe that the energy criterion indicates that for any yield stress Y, most critically equilibrated Bingham fluid ellipsoids are stable to homogeneous perturbations that preserve angular momentum. The maximum dissipation postulate guaranteed stability at first order for all such perturbations except the one which is compatible with the stress state at equilibrium. The compatible perturbation's effect was tested at second order, and led to small regions in the equilibrium landscape being found unstable. Finally, we emphasize that the stability results are applicable to critically equilibrated ellipsoids, i.e., those ellipsoids that lie on the boundary of the equilibrium zone corresponding to their yield stress. It may be shown, by a straightforward

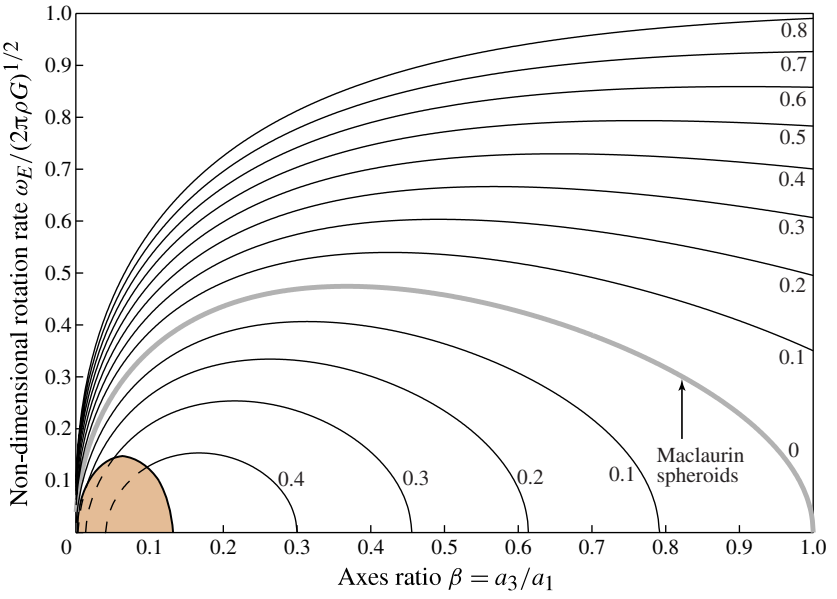

FIGURE 7. (Colour online) Stability of oblate Bingham fluid ellipsoids with $\alpha = 1$. Critically equilibrated ellipsoids lying outside the shaded region are secularly stable for all angular momentum preserving homogeneous perturbations; cf. figure 3.

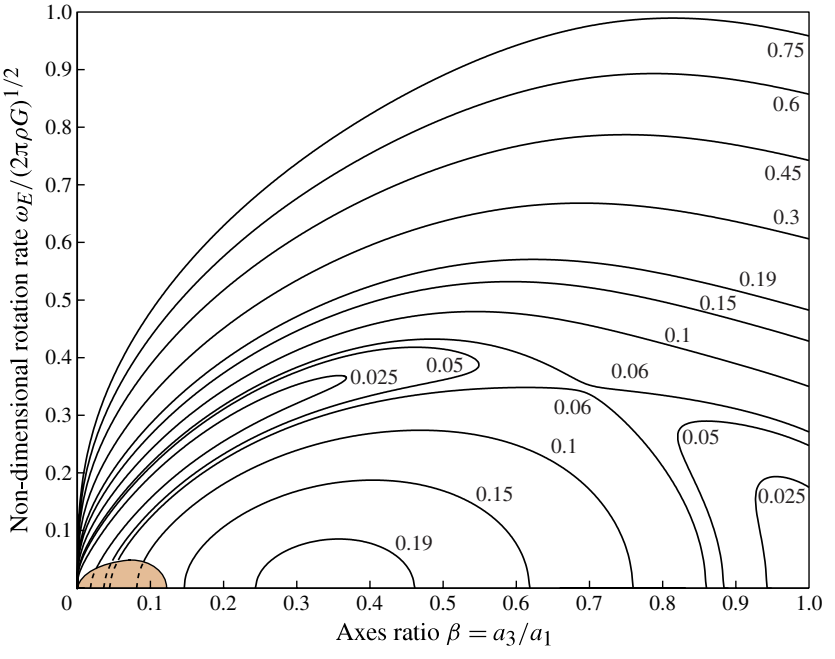

FIGURE 8. (Colour online) Stability of prolate Bingham fluid ellipsoids with $\alpha = \beta$; cf. figure 4. See also figure 7's caption.

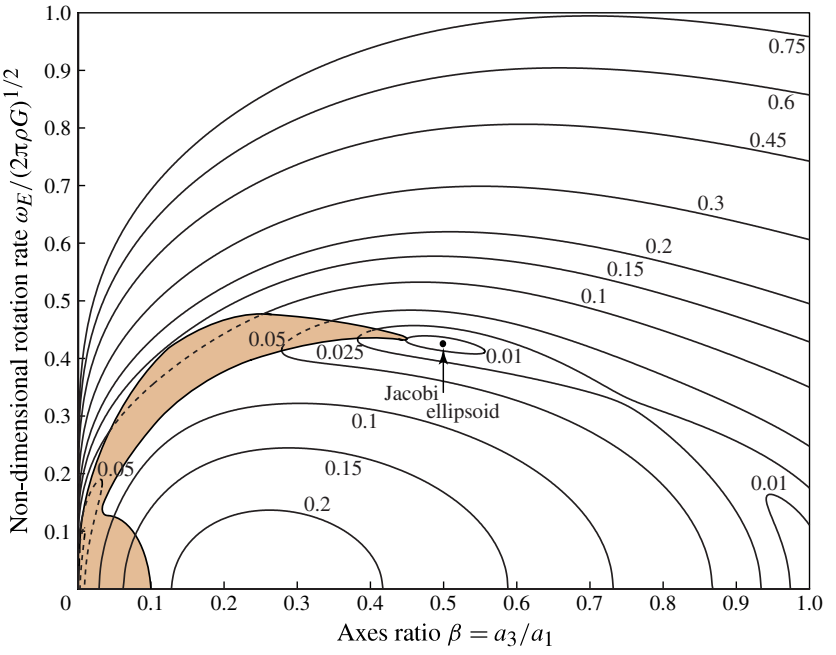

FIGURE 9. (Colour online) Stability of average triaxial Bingham fluid ellipsoids with $\alpha = (1 + \beta)/2$; cf. figure 5. See also figure 7's caption.

application of the maximum dissipation theorem, that ellipsoids that are situated in the interior of their associated equilibrium region are stable at first order to all angular momentum preserving perturbations. This is in marked contrast to inviscid fluids.

The maximum dissipation postulate required that strain rates be normal to the yield surface. This prescription is not always acceptable, as, e.g., in granular materials, where this assumption leads to unrealistic predictions for dilatation. In such cases, where strain rates need not be normal to the yield surface, the maximum dissipation postulate cannot guarantee stability at first order and, indeed, there is a strong contrapositive indication. Alternatively, shear-thinning Bingham fluids, while having a yield surface, tend to flow post-yield akin to low-viscosity fluids. In the limit, we may imagine a Bingham fluid that post-yield flows in the same way as an inviscid fluid, and we may model this by having the cylinder representing the yield surface (3.7) collapse onto its axis immediately after yielding. Such a limit may be relevant for, say, a strongly dilating granular aggregate, as internal friction will drastically reduce when the aggregate's density reduces. Indeed, internal friction in a granular material has both interfacial and geometric roots. The latter dictates how closely packed is the material. As in the case of inviscid fluids, δE_k's sign is now regulated by $\delta^{(2)}E_k$ given by (5.2) with all perturbations that keep $\boldsymbol{H}_p$ zero now being permitted. Thus, the toroidal mode $D_{11} = -D_{22} = 1$ is the most unstable. Figures 10–12 display the results of the stability analysis. We observe that the stability zones are greatly reduced. This is intuitively reasonable as shear thinning should have a destabilizing effect. In figure 10, as expected, the stability boundary now passes through the Jacobi point wherefrom the Jacobi ellipsoids

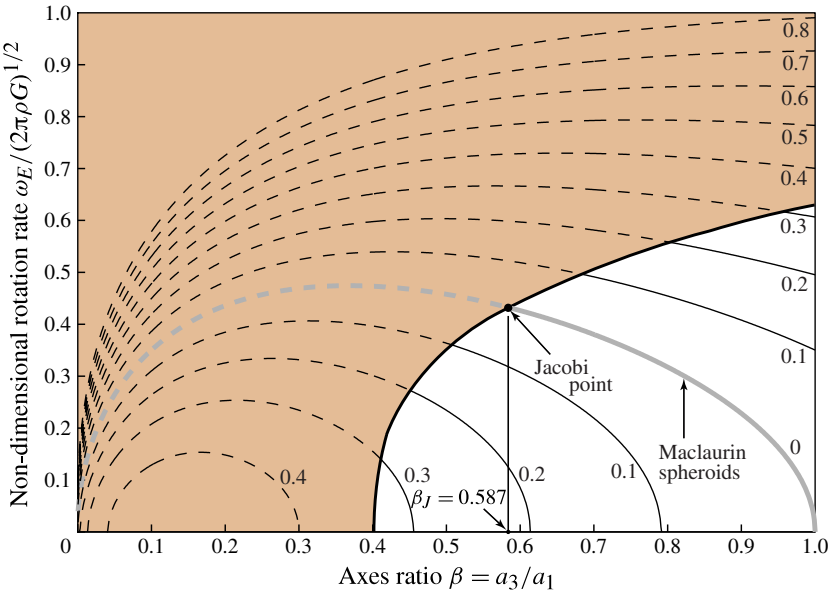

FIGURE 10. (Colour online) Stability of oblate infinitely fast shear-thinning Bingham fluid ellipsoids with $\alpha = 1$ that post-yield flow as inviscid fluids. Critically equilibrated ellipsoids lying outside the shaded region are secularly stable for all angular momentum preserving homogeneous perturbations; cf. figures 3 and 7.

branch from the Maclaurin sequence. Similarly, in figure 12 the stability boundary misses the point where the Jacobi sequence meets the plane $\alpha = (1 + \beta)/2$, as it must, given that § 5.1.2's analysis predicted Jacobi ellipsoids to be stable in the frame $\mathscr{O}$.

6. Conclusion

In this work, we have developed a general test for the secular stability of rotating non-smooth complex fluids. Bingham fluids offer a first example of such non-smooth systems. Projecting the dynamics on to the finite-dimensional space of homogeneous motions, the stability test was first applied to the classical problem of rotating self-gravitating inviscid fluid ellipsoids. Inviscid fluids may be obtained from Bingham fluids in the limit of the yield stress going to zero. In the process, we clarified several issues that have not been made clear in previous applications of the energy criterion to inviscid fluids. We gave a precise definition of the rotating coordinate frame $\mathscr{O}$ in which to apply the energy criterion. We also differentiated between perturbations that preserved relative angular momentum in $\mathscr{O}$, and those that added angular momentum. We saw that the energy criterion gave results in line with previous energy and spectral analyses only in the former case. This fact has not previously been highlighted, although Lebovitz (1966) and Hunter (1977) hint at this in passing. Next, we explained why in contrast to Chandrasekhar's (1969) spectral analysis, and the present and earlier applications of the energy criterion, Riemann's (1860) analysis that was also predicated on energy methods, recovered the Riemann point β_R, and not the Jacobi point β_J, as the point where secular instability sets in. The reason lay in Riemann's choice of $\sum \dot{a}_i^2$, as opposed to E_k given by (4.17), as a measure of a homogeneously deforming ellipsoid's 'kinetic energy'.

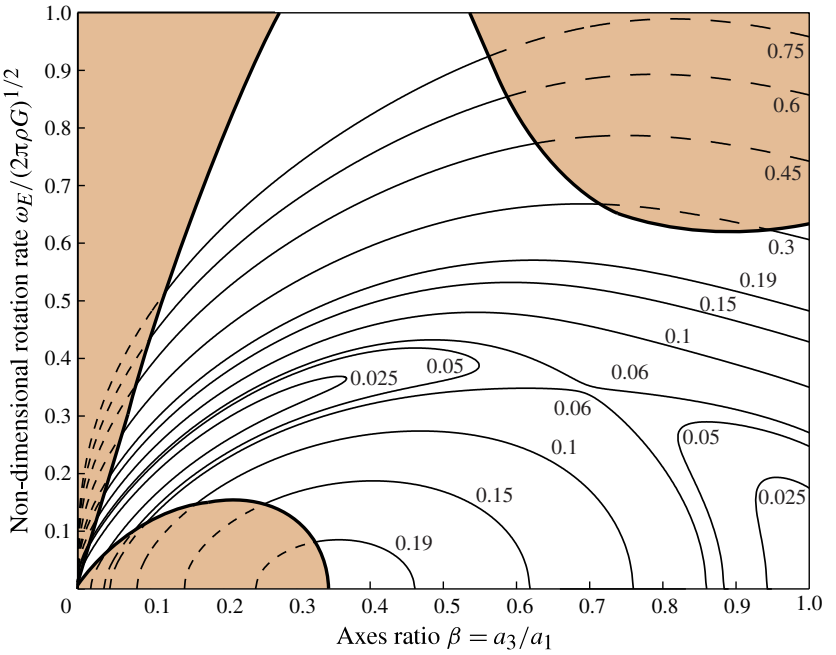

FIGURE 11. (Colour online) Stability of prolate infinitely fast shear-thinning Bingham ellipsoids with $\alpha = \beta$; cf. figures 4 and 8. See also the caption to figure 10.

We then explored the equilibrium shapes and stability of freely rotating self-gravitating Bingham fluid ellipsoids. We saw that the presence of a non-zero yield stress greatly expanded the possible equilibrium shapes. However, the non-smooth nature of the underlying constitutive law made spectral stability analysis inapplicable and we had to extend the energy criterion to such systems. As before, the Bingham fluid ellipsoids were secularly unstable for perturbations that added angular momentum $\boldsymbol{H}_p$. Restricting ourselves to perturbations for which $\boldsymbol{H}_p$ was zero, we still had to distinguish between compatible and incompatible perturbations for materials with a yield surface, with the maximum dissipation postulate assuring us of first-order stability in the latter case. Consequently, most equilibrium shapes were stable to angular momentum preserving perturbations; narrow secularly unstable regions were identified by compatible perturbations. By way of contrast, and to also explore the effects of shear thinning, we probed the stability of infinitely fast shear-thinning Bingham fluids. As one may expect, the stability zones were greatly reduced for such materials.

A motivation for investigating the stability of non-smooth materials such as Bingham fluids was the increasing acceptance of the fact that several small planetary bodies may be rubble piles held together by internal gravity. As mentioned in the Introduction, pressure-dependent Bingham fluids are often employed as a first model for granular aggregates. The general stability criterion developed here may, with appropriate modifications, be applied to any rotating non-smooth complex fluid, and is currently being extended to pressure-dependent materials in the context of the structural stability of rubble asteroids.

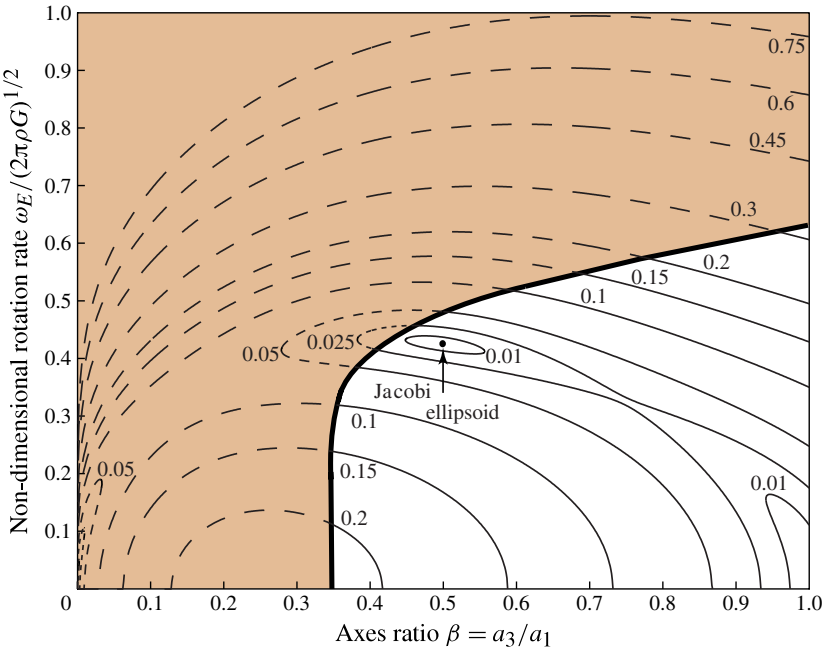

FIGURE 12. (Colour online) Stability of average triaxial infinitely fast shear-thinning Bingham ellipsoids with $\alpha = (1 + \beta)/2$; cf. figures 5 and 9. See also the caption to figure 10.

Acknowledgements

I thank S. Mahesh, V. Shankar, A. Chatterjee, M. K. Verma, S. L. Das, P. Wahi and A. Chatterjee of the Mechanics & Applied Mathematics Group at IIT Kanpur, and A. K. Mallik of Bengal Engineering College, Shibpur for helpful discussions. I am also grateful to B. S. Jang of UNIST, South Korea for his hospitality on my visits there during which much of this work was done.

Appendix A. Computing $\dot{\boldsymbol{A}}$

In the ellipsoid's principal axes coordinate system $\hat{\boldsymbol{\imath}}_i$,

$$\boldsymbol{I} = \sum_{i=1}^{3} I_i \hat{\boldsymbol{\imath}}_i \otimes \hat{\boldsymbol{\imath}}_i \quad \text{and} \quad \boldsymbol{A} = \sum_{i=1}^{3} A_i \hat{\boldsymbol{\imath}}_i \otimes \hat{\boldsymbol{\imath}}_i. \tag{A 1}$$

Thus, taking the time derivative in the rotating frame $\mathscr{O}$, we find

$$\dot{\boldsymbol{A}} = \sum_{i=1}^{3} \left(\dot{A}_i \hat{\boldsymbol{\imath}}_i \otimes \hat{\boldsymbol{\imath}}_i + A_i \dot{\hat{\boldsymbol{\imath}}}_i \otimes \hat{\boldsymbol{e}}_i + A_i \hat{\boldsymbol{\imath}}_i \otimes \dot{\hat{\boldsymbol{\imath}}}_i \right). \tag{A 2}$$

Because $\hat{\boldsymbol{\imath}}_i$ are unit vectors identifying a Cartesian coordinate system, we write

$$\dot{\hat{\boldsymbol{\imath}}}_i = \boldsymbol{O} \cdot \hat{\boldsymbol{\imath}}_i, \tag{A 3}$$

where $\boldsymbol{O}$ is the angular velocity tensor associated with the ellipsoid's principal axes' rotation with respect to $\mathscr{O}$ that, recall, rotates at $\boldsymbol{\omega}(t)$ to keep the relative angular

momentum constant. To find $\boldsymbol{O}$, we differentiate $\boldsymbol{I}$ given above, employ (A 3), equate the expression to $\dot{\boldsymbol{I}}$ given by (2.15) and separate the diagonal and off-diagonal parts to find

$$\dot{a}_i = a_i D_{ii} \quad \text{(no sum)} \tag{A 4a}$$

$$O_{ij} = -W_{ij} - \frac{a_i^2 + a_j^2}{a_i^2 - a_j^2} D_{ij}, \quad (a_i \neq a_j). \tag{A 4b}$$

The first of the above provide the rate of change of the ellipsoid's semi-major axes in terms of the strain rate gradient $\boldsymbol{D}$. As expected, $\boldsymbol{W}$, the spin part of $\boldsymbol{L}$, has no effect on $\dot{a}_i$. When $a_i = a_j$ the corresponding component of $\boldsymbol{O}$ appears to have a singularity. We resolve this by invoking in-plane symmetry that allows us to select $\hat{\boldsymbol{i}}_i$ and $\hat{\boldsymbol{i}}_j$ so that D_{ij} vanishes, allowing a limit to be taken. The limiting value may be found by requiring that $\dot{O}_{ij}$ be finite.

To compute $\dot{A}_i$, we note from (2.11) that A_i are functions only of axes' ratios, so that

$$\dot{A}_i = \frac{\partial A_i}{\partial \alpha}\dot{\alpha} + \frac{\partial A_i}{\partial \beta}\dot{\beta}, \tag{A 5}$$

and with some effort, utilizing formulae for A_i in (2.11), we evaluate

$$\frac{\partial A_1}{\partial \alpha} = \frac{2\beta}{1-\alpha^2}\left\{\frac{\alpha\beta}{\alpha^2-\beta^2} + \frac{\sqrt{1-\beta^2}}{1-\alpha^2}\left(\frac{\alpha^2 E[r,s]}{\alpha^2-\beta^2} + \frac{E[r,s] - (1+\alpha^2)F[r,s]}{1-\beta^2}\right)\right\}, \tag{A 6a}$$

$$\frac{\partial A_3}{\partial \alpha} = \frac{2\beta\sqrt{1-\beta^2}}{(\alpha^2-\beta^2)^2}\left\{-\frac{2\alpha\beta}{\sqrt{1-\beta^2}} + \frac{\alpha^2 E[r,s]}{1-\alpha^2} + \frac{\beta^2 E[r,s]}{1-\beta^2} - \frac{\alpha^2(\alpha^2-\beta^2)F[r,s]}{(1-\alpha^2)(1-\beta^2)}\right\} \tag{A 6b}$$

$$\frac{\partial A_1}{\partial \beta} = \frac{2\alpha}{1-\beta^2}\left\{\frac{-\alpha\beta}{\alpha^2-\beta^2} + \frac{1}{\sqrt{1-\beta^2}}\left(\frac{\beta^2 E[r,s]}{\alpha^2-\beta^2} - \frac{E[r,s] - F[r,s]}{1-\alpha^2}\right)\right\}, \tag{A 6c}$$

and

$$\frac{\partial A_3}{\partial \beta} = \frac{2\alpha}{\alpha^2-\beta^2}\left\{\left(\frac{\beta}{1-\beta^2} + \frac{2\beta}{\alpha^2-\beta^2}\right)\left(\alpha - \frac{\beta E[r,s]}{\sqrt{1-\beta^2}}\right) - \frac{E[r,s] - \beta^2 F[r,s]}{(1-\beta^2)^{3/2}}\right\}. \tag{A 6d}$$

In the above formulae, taking the limit $\alpha \to 1$ we obtain

$$\frac{\partial A_1}{\partial \alpha} = \frac{\beta}{4}\left\{\frac{\beta(1+2\beta^2)}{(1-\beta^2)^2} + \frac{1-4\beta^2}{(1-\beta^2)^{5/2}}\sin^{-1}\sqrt{1-\beta^2}\right\}, \tag{A 7a}$$

$$\frac{\partial A_2}{\partial \alpha} = \frac{\beta}{4}\left\{\frac{\beta(11-2\beta^2)}{(1-\beta^2)^2} - \frac{5+4\beta^2}{(1-\beta^2)^{5/2}}\sin^{-1}\sqrt{1-\beta^2}\right\}, \tag{A 7b}$$

and

$$\frac{\partial A_1}{\partial \beta} = \frac{\partial A_2}{\partial \beta} = -\frac{3\beta}{(1-\beta^2)^2} + \frac{1+2\beta^2}{(1-\beta^2)^{5/2}}\sin^{-1}\sqrt{1-\beta^2} \tag{A 7c}$$

that are to be employed for oblate ellipsoids, while the limit $\alpha \to \beta$ yields results appropriate for prolate objects:

$$\frac{\partial A_1}{\partial \alpha} = \frac{\partial A_1}{\partial \beta} = -\frac{3\beta}{(1-\beta^2)^2} + \frac{1+2\beta^2}{(1-\beta^2)^{5/2}} \tanh^{-1}\sqrt{1-\beta^2} \tag{A 8a}$$

and

$$\frac{\partial A_3}{\partial \alpha} = \frac{\partial A_2}{\partial \beta} = \frac{\beta}{4}\left\{\frac{2+\beta^2}{\beta\,(1-\beta^2)^2} - \frac{4-\beta^2}{(1-\beta^2)^{5/2}} \tanh^{-1}\sqrt{1-\beta^2}\right\}. \tag{A 8b}$$

In each case above, the missing partial derivatives may be obtained by differentiating identity (2.12). Note that, from (A 4*a*) and their definitions, we easily show that

$$\dot{\alpha} = \alpha\,(D_{22} - D_{11}) \quad \text{and} \quad \dot{\beta} = \beta\,(D_{33} - D_{11})\,. \tag{A 9}$$

Thus, finally, employing rates $\dot{A}_i$ available from (A 5) along with one of (A 6), (A 7), or (A 8), $\dot{\alpha}$ and $\dot{\beta}$ from (A 9), and $\boldsymbol{O}$'s components from (A 4*b*), respectively, we may compute

$$\dot{\boldsymbol{A}} = \sum_{i=0}^{3} \dot{A}_i \hat{\boldsymbol{i}}_i \otimes \hat{\boldsymbol{i}}_i + \boldsymbol{O}\cdot\boldsymbol{A} - \boldsymbol{A}\cdot\boldsymbol{O}. \tag{A 10}$$

REFERENCES

ABRAMOWITZ, M. & STEGUN, I. A. 1965 *Handbook of Mathematical Functions*. Dover.

BOTTKE, W. F. JR., CELLINO, A., PAOLICCHI, P. & BINZEL, R. P. 2002 An overview of the asteroids: the asteroids III perspective. In *Asteroids III* (ed. W. F. Bottke JR., A. Cellino, P. Paolicchi & R. P. Binzel), pp. 3–15. University of Arizona Press.

BURNS, J. A. & SAFRONOV, V. S. 1973 Asteroid nutation angles. *Mon. Not. R. Astron. Soc.* **165**, 403–411.

CHAKRABARTY, J. 1969 On uniqueness and stability in rigid/plastic solids. *Intl J. Mech. Sci.* **11** (9), 723–731.

CHANDRASEKHAR, S. 1969 *Ellipsoidal Figures of Equilibrium*. Yale University Press.

CHEN, W. F. & HAN, D. J. 1988 *Plasticity for Structural Engineers*. Springer.

GREENWOOD, D. T. 1988 *Principles of Dynamics*. Prentice-Hall.

HAGIHARA, Y. 1970 *Theories of Equilibrium Figures of a Rotating Homogeneous Fluid Mass*. US Government Printing Office.

HARRIS, A. W., FAHNESTOCK, E. G. & PRAVEC, P. 2009 On the shapes and spins of 'rubble pile' asteroids. *Icarus* **199**, 310–318.

HILL, R 1957 Stability of rigid-plastic solids. *J. Mech. Phys. Solids* **6** (1), 1–8.

HOLSAPPLE, K. A. 2001 Equilibrium configurations of solid cohesionless bodies. *Icarus* **154**, 432–448.

HOLSAPPLE, K. A. 2007 Spin limits of solar system bodies: from the small fast-rotators to 2003 EL61. *Icarus* **187**, 500–509.

HUNTER, C 1977 On secular stability, secular instability, and points of bifurcation of rotating gaseous masses. *Astrophys. J.* **213**, 497.

JARDETZKY, W. 1958 *Theories of Figures of Celestial Bodies*. Interscience.

JEANS, J. H. 1961 *Astronomy and Cosmogony*, 2nd ed. Dover.

JOP, P., FORTERRE, Y. & POULIQUEN, O. 2006 A constitutive law for dense granular flows. *Nature* **441**, 727–730.

KELLOGG, O. D. 1953 *Foundations of Potential Theory*. Dover.

KNOPS, R. J. & WILKES, E. W. 1966 On Movchan's theorems for stability of continuous systems. *Intl J. Engng Sci.* **4**, 303–329.

KNOPS, R. J. & WILKES, E. W. 1973 Theory of elastic stability. In *Encyclopedia of Physics Vol. VI a/3: Mechanics of Solids* (ed. S. Flügge), pp. 125–302. Springer.

KOITER, W. T. 2008 *Elastic Stability of Solids and Structures*. Cambridge University Press.

LAI, D., RASIO, F. A. & SHAPIRO, S. L. 1993 Ellipsoidal figures of equilibrium: compressible models. *Astrophys. J. Suppl.* S **88**, 205–252.

LASALLE, J. & LEFSCHETZ, S. 1961 *Stability by Lyapunov's Direct Method*. Academic.

LEBOVITZ, N. R. 1966 On Riemann's criterion for the stability of liquid ellipsoids. *Astrophys J.* **145**, 878.

LEBOVITZ, N. R. 1998 The mathematical development of the classical ellipsoids. *Intl J. Engng Sci.* **36**, 1407–1420.

LUBLINER, JACOB 1990 *Plasticity Theory*. Macmillan.

LYTTLETON, R. A. 1953 *The Stability of Rotating Liquid Masses*. Cambridge University Press.

MOVCHAN, A. A. 1959 Direct method of Liapunov in stability problems of elastic systems. *J. Appl. Math. Mech.* **23**, 483–493.

MOVCHAN, A. A. 1960 Stability of processes with respect to two metrics. *J. Appl. Math. Mech.* **24**, 988–1001.

MUNK, W. H. & MACDONALD, G. J. F. 1960 *The Rotation of the Earth*. Cambridge University Press.

NGUYEN, Q. S. 2000 *Stability and Nonlinear Solid Mechanics*. John Wiley & Sons.

OLDROYD, J. G. 1947 A rational formulation of the equations of plastic flow for a Bingham solid. *Math. Proc. Cambridge* **43**, 100–105.

PRAGER, W. 1961 *Introduction to Mechanics of Continua*. Ginn & Co.

RICHARDSON, D. C., ELANKUMARAN, P. & SANDERSON, R. E. 2005 Numerical experiments with rubble piles: equilibrium shapes and spins. *Icarus* **173**, 349–361.

RICHARDSON, D. C., LEINHARDT, Z. M., MELOSH, H. J., BOTTKE, W. F. JR. & ASPHAUG, E. JR. 2002 Gravitational aggregates: evidence and evolution. In *Asteroids III* (ed. W. F. Bottke, A. Cellino, P. Paolicchi & R. P. Binzel), pp. 501–515. University of Arizona Press.

RIEMANN, B. 1860 Ein Beitrag zu den Untersuchengen über die Bewegung eines flüssigen gleichartigen Ellipsoides. *Königl. Gesell. Wis. zu Göttingen* **8**.

ROSENKILDE, C. E. 1967 The tensor virial-theorem including viscous stress and the oscillations of a Maclaurin spheroid. *Astrophys. J.* **148**, 825–841.

SANCHEZ, P. & SCHEERES, D. J. 2012 DEM simulation of rotation-induced reshaping and disruption of rubble-pile asteroids. *Icarus* **218**, 876–894.

SHARMA, I., BURNS, J. A. & HUI, C.-Y. 2005 Nutational damping times in solids of revolution. *Mon. Not. R. Astron. Soc.* **359**, 79–92.

SHARMA, I., JENKINS, J. T. & BURNS, J. A. 2009 Dynamical passage to approximate equilibrium shapes for spinning, gravitating rubble asteroids. *Icarus* **200**, 304–322.

STORÅKERS, B. 1977 On uniqueness and stability under configuration-dependent loading of solids with or without a natural time. *J. Mech. Phys. Solids* **25** (4), 269–287.

ZIEGLER, H. 1968 *Principles of Structural Stability*. Blaisdell Pub. Co.